Sulfur isotopic signature of Earth established by planetesimal volatile evaporation

Wenzhong Wang[1,2,3,*], Chun-Hui Li[4,5,*], John P. Brodholt[2,6], Shichun Huang[7], Michael J. Walter[3], Min Li[8], Zhongqing Wu[1,9,10], Fang Huang[5,9], Shui-Jiong Wang[11]

[1]Laboratory of Seismology and Physics of Earth's Interior, School of Earth and Space Sciences, University of Science and Technology of China, Hefei, Anhui 230026, China

[2]Department of Earth Sciences, University College London, London WC1E 6BT, United Kingdom

[3]Earth and Planets Laboratory, Carnegie Institution for Science, Washington, DC 20015, USA

[4]International Center for Planetary Science, College of Geosciences, Chengdu University of Technology, Chengdu 610059, China

[5]CAS Key Laboratory of Crust-Mantle Materials and Environments, School of Earth and Space Sciences, University of Science and Technology of China, Hefei, Anhui 230026, China

[6]Centre for Earth Evolution and Dynamics, University of Oslo, Oslo, Norway

[7]Department of Geoscience, University of Nevada, Las Vegas, United States

[8]Department of Physics and Astronomy, University of Nevada, Las Vegas

[9]CAS Center for Excellence in Comparative Planetology, USTC, Hefei, Anhui 230026, China

[10]National Geophysical Observatory at Mengcheng, USTC, Hefei, China

[11]State Key Laboratory of Geological Processes and Mineral Resources, China University of Geosciences, Beijing, China.

[*]Correspondence and requests for materials should be addressed to W.W. (wenzhong.wang@ucl.ac.uk) and C.-H.L. (lichunhui@cdut.edu.cn).

Abstract

How and when Earth's volatile content was established is controversial with several mechanisms postulated, including planetesimal evaporation, core formation, and the late delivery of undifferentiated chondrite-like materials. The isotopes of volatile elements such as sulfur can be fractionated during planetary accretion and differentiation, and thus are potential tracers of these processes. Using first-principles calculations, we examine sulfur isotope fractionation during core formation and planetesimal evaporation. We find no measurable sulfur isotope fractionation between silicate and metallic melts at core-forming conditions, indicating that the observed light sulfur isotope composition of the bulk silicate Earth relative to chondrites cannot be explained by metal-silicate fractionation. Our thermodynamic calculations show that sulfur evaporates mostly as H_2S during planetesimal evaporation when nebular H_2 is present. The observed bulk Earth sulfur isotope signature and abundance can be reproduced by the evaporative loss of ~90% sulfur mainly as H_2S from molten planetesimals before nebular H_2 is dissipated. The heavy sulfur isotope composition of the Moon relative to the Earth is consistent with evaporative sulfur loss under 94-98% saturation condition during the Moon-forming giant impact. In summary, volatile evaporation from molten planetesimals prior to Earth's formation likely played a key role in establishing Earth's volatile element content.

Understanding the accretion history of Earth's volatile elements, such as sulfur (S), carbon (C), hydrogen (H) and nitrogen (N), is of profound importance for understanding planetary formation, evolution, and habitability. Earth formed from protoplanetary embryos with chemical compositions assumed to be similar to undifferentiated chondrites[1]. Compared with the solar composition and primitive chondrites, the bulk silicate Earth (BSE) has a similar refractory lithophile element abundance pattern but is strongly depleted in volatile elements[2]. Different interpretations have been proposed to explain this strong volatile element depletion. For instance, the depletion pattern could be explained qualitatively by the late accretion of 10-20% of a volatile-rich body to a volatile-depleted proto-Earth[3]. Partial melting and vaporization on bodies heated by the decay of short-lived nuclei[4], such as ^{26}Al, may have caused extensive volatile loss in the protoplanetary embryos that formed Earth[5,6]. Depletion of some siderophile (iron-loving) elements, such as S, may also be associated with core-mantle differentiation[7–9] and/or the Hadean sulfide segregation into the core[10]. However, a recent study[11] argued that the volatile depletion in the BSE was inherited from a carbonaceous chondrite-like source, suggesting that exotic addition of materials or vaporization from Earth's precursors are not strictly required.

The abundance of volatiles and their isotopic compositions are commonly used to distinguish between different mechanisms for establishing a volatile depleted mantle. Sulfur, selenium (Se), and tellurium (Te) are highly siderophile elements with similar and relatively low 50% condensation temperatures in a solar nebula composition gas[12]. Measurements of S, Se, and Te abundances in mantle peridotites suggest that a volatile-rich late veneer of carbonaceous-chondrite-like material is required to explain the relative ratios of S, Se and Te in the BSE[13], but it is debated whether peridotites preserve primitive mantle signatures[14]. The BSE has an average stable S isotope composition (expressed as $\delta^{34}S = [(^{34}S/^{32}S)_{sample}/(^{34}S/^{32}S)_{CDT} - 1] \times 1000$ ‰ and CDT is Canyon Diablo Troilite) of -1.40 ± 0.50‰ (1SD)[15,16], which is significantly lower than the average chondritic values[17–19] (Fig. 1). Labidi et al.[15,16] argued that core-mantle differentiation[7,8], rather than a late veneer, was responsible for the sub-chondritic $\delta^{34}S$ of the BSE. Equilibrium S isotope fractionation factors at core-forming conditions are required to test this hypothesis, however, to date such data are not well constrained. Published experiments[20] on S isotope fractionation between metal and silicate melt have been performed only at < 2 GPa and < 2000 K, whereas the pressure and temperature (P-T) for Earth's core formation are expected to be much higher[21]. Both experimental and theoretical studies[22–24] demonstrate that the structure of silicate melts changes dramatically with pressure, indicating that metal-silicate S isotopic fractionation measured at low pressure cannot be directly applied to high-pressure core formation[20].

As a volatile element, S would have undergone significant vaporization during Earth's accretion like other moderately volatile elements[5] such as Bi, Sn, Pb, and Zn. Previous studies have investigated S isotope fractionation during evaporation from troilite[25], and Mg and Si isotope fractionation during planetesimal evaporation[6,26], but the effect of evaporation on S isotopes from planetesimals is unexplored. Whether the sub-chondritic δ^{34}S of the BSE is related to S loss during early vaporization from Earth's precursor bodies fundamentally impacts our understanding of the volatile depletion in the BSE.

Structural properties of sulfur in melts

Here we present first-principles calculations that constrain the equilibrium S isotope fractionation between silicate and metallic melts, and between the vapor phase and silicate melt. We first conducted first-principles molecular dynamics (FPMD) simulations based on density functional theory (DFT) (see Methods) to obtain the structures of S-bearing silicate and metallic melts at 4-105 GPa and 3000 K. The structural information of S shows a large difference under relatively reducing and oxidizing conditions. Under relatively oxidizing conditions ($Mg_{32}Si_{32}O_{96}SO_2$), S is directly bonded to O to form sulfate with a short S-O distance of ~ 1.5 Å (Extended Data Fig. 1). In contrast, S is bonded to Fe, Mg and/or Si in $Mg_{32}Si_{32}O_{95}S$ and $Mg_{41}Ca_2Fe_5Si_{32}Al_4O_{117}S$ melts (Extended Data Fig. 2), which correspond to relatively reducing conditions. In $Fe_{97}S_3$ and $Fe_{87}Ni_4Si_{10}O_2C_2S_3$ melts, S is dominantly bonded to Fe and/or Ni with a S-Fe/Ni distance of ~2.1 Å (Extended Data Fig. 3 and 4).

The average force constants <*F*> of S in silicate and metallic melts (Extended Data Fig. 5 and Supplementary Table 1) were estimated using the small displacement method based on the harmonic approximation (see Methods and supporting materials).

The <*F*> values of S are dominated by structural properties such as bond lengths. For instance, the <*F*> of S in the $Mg_{32}Si_{32}O_{96}SO_2$ melt is much larger than those in $Mg_{32}Si_{32}O_{95}S$, $Mg_{41}Ca_2Fe_5Si_{32}Al_4O_{117}S$, $Fe_{87}Ni_4Si_{10}O_2C_2S_3$, and $Fe_{97}S_3$ melts, which can be explained by the much shorter S-O distance in $Mg_{32}Si_{32}O_{96}SO_2$ than the S-Mg/Fe/Si/Ni distances in melts under relatively reducing conditions. In contrast, the <*F*> of S in reducing silicate melts ($Mg_{32}Si_{32}O_{95}S$ and $Fe_{87}Ni_4Si_{10}O_2C_2S_3$) are slightly larger than those in metallic melts ($Fe_{97}S_3$ and $Fe_{87}Ni_4Si_{10}O_2C_2S_3$), although this difference becomes somewhat greater at > 80 GPa. Both silicate and metallic melts become substantially more packed with increasing compression and hence, their S force constants increase significantly with pressure. Compared with $Mg_{32}Si_{32}O_{95}S$ and $Fe_{97}S_3$ melts, the <*F*> of S in $Mg_{41}Ca_2Fe_5Si_{32}Al_4O_{117}S$ and $Fe_{87}Ni_4Si_{10}O_2C_2S_3$ melts only increase by ~15 N/m (Extended Data Fig. 5).

Sulfur isotope fractionation during core formation

Using the high-temperature approximation of the Bigeleisen–Mayer equation[27], we calculated the reduced partition function ratio ($10^3\ln\beta$ or β factor) of $^{34}S/^{32}S$ from the <*F*> (Extended Data Fig. 6) and the equilibrium S isotope fractionation factors ($10^3\ln\alpha$) between silicate and metallic melts at different pressures (Fig. 2). Our results demonstrate that the oxidizing $Mg_{32}Si_{32}O_{96}SO_2$ silicate melt is enriched in ^{34}S relative to metallic melts, but there is no measurable equilibrium S isotope fractionation between the reducing silicate and metallic melts within the range of < 80 GPa. The substantial changes in melt structural properties under compression only mildly affect the $10^3\ln\alpha$ between silicate and metallic melts. At 3000 K and 0-90 GPa, the $10^3\ln\alpha$ between the reducing silicate and metallic melts is smaller than 0.05‰, while the value between $Mg_{32}Si_{32}O_{96}SO_2$ and $Fe_{97}S_3$/$Fe_{87}Ni_4Si_{10}O_2C_2S_3$ is 0.35±0.02 ‰. Thus, the S isotope fractionation between the mantle and core is dominated by the S speciation in the silicate melt.

The speciation of S in silicate melt is strongly controlled by the oxygen fugacity

(fO_2)[28,29]. At log fO_2 < FMQ-1 (1 log unit lower than the Fayalite–Magnetite–Quartz buffer), S^{2-} is the dominant species; at log fO_2 > FMQ+2, S occurs as S^{6+}, whereas at FMQ-1 < log fO_2 < FMQ+2, S^{2-} and S^{6+} coexist, and S^{6+} content increases sharply with log fO_2. Under the redox conditions of core formation for Earth, Mars, and Moon (< FMQ-4)[30,31], S^{2-} should be the dominant species in silicate melt, and our results show no measurable S isotope fractionation between silicate and metallic melts is predicted (Fig. 2), and this conclusion is independent of the pressure of core formation[2,32]. Calculations using two endmember models (equilibrium and Rayleigh distillation)[2,33,34] show that core-mantle differentiation can only cause a very small positive shift of +0.02-0.1‰ in $\delta^{34}S$ of the silicate mantle (Fig. 2c), which cannot explain the negative $\delta^{34}S$ of the BSE relative to chondrites (Fig. 1).

Mechanisms for sulfur isotope signatures in Earth and Moon

In addition to ruling out core formation as the cause of the negative $\delta^{34}S$ of the BSE, the very small fractionation of S isotopes caused by core formation means that metallic cores have similar S isotopic ratios to their silicate mantles. Consequently, the measured BSE isotopic composition[15] of -1.40 ± 0.50‰ should be representative of the bulk Earth. Such a negative $\delta^{34}S_{Earth}$ cannot be explained by late delivery of S to the BSE[11,35,36] because most late-veneer materials have heavier $\delta^{34}S$ than the Earth (Fig. 1). Although the negative $\delta^{34}S$ of CM chondrites could be as low as -1.11± 0.30 ‰, most CM chondrites are characterized by a non-zero $\Delta^{33}S$ (from -0.005 ± 0.02 ‰ to 0.213 ± 0.02 ‰; $\Delta^{33}S = 1000 \times [\delta^{33}S - [(\delta^{34}S + 1)^{0.515} - 1]]$ ‰), which is inconsistent with the zero $\Delta^{33}S$ measured in terrestrial MORB (0.005 ± 0.008 ‰)[19]. The average $\Delta^{33}S$ and $\delta^{34}S$ values of CM chondrites[19] are 0.021 ± 0.068 ‰ and -0.08 ± 0.44‰, respectively, which could produce zero $\Delta^{33}S$ but cannot reproduce the $\delta^{34}S_{Earth}$ value. We therefore now consider whether this sub-chondritic $\delta^{34}S_{Earth}$ may be associated with volatile loss during Earth's accretion.

Small precursor bodies with heat sources such as radiogenic ^{26}Al[4] would have undergone partial melting and vaporization, in which gravitational escape of volatiles is possible if these precursor bodies have relatively small radii (< 1000 km)[26]. Our thermodynamic calculations (see Methods) show that S mainly occurs as H_2S in the vapor phase (Supplementary Table 2) in the presence of nebular H_2 with a total pressure of about 10^{-4} bar[12,37]. Under such conditions, the net fractionation as a consequence of planetesimal evaporation would be equal to the equilibrium isotope fractionation between vapor phase and melt[26]. This kind of planetesimal evaporation can explain the concentrations of Mg and Si and their isotopic signatures of the bulk Earth[26]. Combining the fractions of each major S species with their $<F>$ (Supplementary Table 1), we estimated the equilibrium vapor-melt S isotope fractionation ($\Delta^{34}S^{eq}_{\text{vapor-melt}}$) to be ~+0.45‰ at 1400 K (Extended Data Fig. 7). Therefore, S evaporation from planetesimal melts would enrich the melt phase with light S isotopes. About 90% loss of S can explain the $\delta^{34}S$ difference between the bulk Earth and chondrites (Fig. 3). This S evaporation process would leave a bulk Earth accreted from enstatite-chondritic materials (3.3-5.8 wt% S, Wang and Becker[13]) with a S concentration of 3300-5800 ppm. Such an initial S concentration can reproduce the S abundance of the BSE[38] after S sequestration into the core[7,9] without a contribution from a late veneer.

While our model does not require a late veneer, a late delivery of S is still allowed if the amount of S loss during evaporation is greater than 90%. In this case, the proto-Earth would have an even lower $\delta^{34}S$ that would then be increased by the late-veneer addition with a chondrite-like heavier $\delta^{34}S$. The more S is evaporated, the more S is required to be added by a late veneer to match the S abundance in the BSE. However, the $\delta^{34}S$ in the BSE will be close to those of chondrites if the amount of S added by the late veneer is too high, and so to reproduce the S abundance and $\delta^{34}S$ value of the BSE, the amount of S added by a late veneer to the BSE should not exceed ~30% of the present-day BSE's S budget. As such, if the late veneer is characterized by chondrite-like materials with 1.0 wt% S, the mass of late-veneer materials should not exceed 0.4% of Earth's mass, consistent with estimates based on abundances of highly siderophile elements[39].

We can also explain the large $\Delta^{34}S_{\text{Moon-Earth}}$ with the loss of volatile elements during the Moon-forming giant impact (Fig. 3). It was suggested that evaporation of moderately volatile elements under a vapor saturation of ~99% can explain the enrichment of their heavy isotopes in the lunar mantle relative to the BSE[40–42]. A high-energy, high-angular-momentum model[43] suggests that the Moon condensed from a vapor of BSE composition at distances beyond the Roche limit under high temperature (~ 3700 K), Under such conditions, S evaporates as multiple species[44], including S, SO, and SO_2. Because of the high temperature, the $\Delta^{34}S^{eq}_{\text{vapor-melt}}$, which is derived from the $<F>$ differences between all possible S species and silicate melt (Extended Data Fig. 11), is only -0.08–0.2‰. Consequently, the $\Delta^{34}S_{\text{vapor-melt}}$ is controlled by the kinetic S isotope fractionation during free evaporation ($\Delta^{34}S^{kin} = [(32/34)^{1/2} - 1]*1000 = -29.8‰$) and the vapor saturation degree (see Methods). If the S concentration ratio between the primitive lunar mantle[45] and the BSE[38] is used to estimate the fraction of S loss, the $\Delta^{34}S_{\text{vapor-melt}}$ required to explain the $\Delta^{34}S_{\text{Moon-Earth}}$ ranges from -0.64‰ to -1.65‰, corresponding to a vapor saturation degree of 0.941-0.977 (Fig. 3), which is similar to that constrained by the isotopic data of several moderately volatile elements (0.989 ± 0.002)[40]. The small difference may be related to the uncertainties in the estimated lunar $\delta^{34}S$, since S isotopes can be fractionated by magmatic events that complicates the estimation of lunar $\delta^{34}S$[46]. Overall, S evaporation during the Moon-forming event can provide a first-order explanation for the enrichment of heavy S isotopes in the Moon.

In conclusion, we show that core formation does not significantly fractionate S isotopes, and the bulk Earth is enriched in light S isotopes relative to chondrites and the Moon. Evaporative loss of 90% S or greater from planetesimals with H_2S as the major evaporative species in the presence of nebular H_2 with a pressure of about 10^{-4} bar can reproduce the sub-chondritic $\delta^{34}S_{\text{Earth}}$ and the S concentration of the BSE. The large $\Delta^{34}S_{\text{Moon-Earth}}$ can also be explained by S evaporation under vapor-unsaturated conditions (94-98%) during the Moon-forming event (Fig. 4). This work strongly supports the profound role of a melt-vapor reaction[5,6] in establishing Earth's volatile element depletion pattern[2].

Corresponding Author. Wenzhong Wang (wenzhong.wang@ucl.ac.uk; wwang10@carnegiescience.edu) and Chun-Hui Li (lichunhui@cdut.edu.cn).

Acknowledgements: This work is supported by the Strategic Priority Research Program (B) of the Chinese Academy of Sciences (XDB41000000), Natural Science Foundation of China (41925017 and 41721002). W. W. acknowledges support from the UCL-Carnegie Postdoctoral Scholarship. S.H. and M.L. acknowledge support from NSF AST-1910955. Part of calculations were conducted at the Supercomputing Center of the University of Science and Technology of China.

Author contributions: W.W. and C.-H.L. conceived and designed this project. W.W. performed the theoretical calculations. S.H. and M.L. did the GRAINS calculations. W.W. wrote the manuscript with the help of C.-H.L. and all authors contributed to the discussion of the results and revision of the manuscript.

Competing interests. The authors declare no competing interests.

Figure captions

Figure 1. Sulfur isotope compositions ($\delta^{34}S$) of planetary materials. The $\delta^{34}S$ of the BSE is defined by terrestrial mid-ocean ridge basalts[15,16], while the $\delta^{34}S$ of the silicate Moon is defined by mare basalts[47]. The $\delta^{34}S$ of sulfides in shergottites are from Franz et al.[48]. The average $\delta^{34}S$ of Vesta is defined by eucrites and diogenites[49,50]. The $\delta^{34}S$ values of carbonaceous (CI, CV, CO and CM), ordinary, and enstatite chondrites are from Gao and Thiemens[17,18], Labidi et al.[19], and Defouilloy et al.[51]. The average $\delta^{34}S$ of carbonaceous chondrites given by Gao and Thiemens[17,18] is +0.49 ± 0.16 ‰. The average of CM from Labidi et al.[19] is -0.08 ± 0.44 ‰; however, most CM samples have non-zero $\Delta^{33}S$ (mass independent sulfur isotope composition, $\Delta^{33}S = 1000 \times [\delta^{33}S - [(\delta^{34}S + 1)^{0.515} - 1]]$ ‰), reflecting the effect of photochemistry[19]. The average of all chondrites (light grey, -0.20 ± 0.20 ‰) is based on samples with Earth-like $\Delta^{33}S$ values[15,16]. The $\delta^{34}S$ values of iron meteorites and pallasites are from Antonelli et al.[52] and Dottin et al.[53], respectively. Error bars represent ±1σ deviation.

Figure 2. Equilibrium sulfur isotope fractionation factors ($10^3\ln\alpha$ of $^{34}S/^{32}S$) between silicate and metallic melts. (a) temperature dependence of $10^3\ln\alpha_{silicate\text{-}metal}$ at different pressures (b) pressure dependence of $10^3\ln\alpha_{silicate\text{-}metal}$ at different temperatures. $Mg_{32}Si_{32}O_{95}S$ and $Mg_{32}Si_{32}O_{96}SO_2$ represent S-bearing silicate melts under relatively reducing and oxidizing conditions, respectively. Error bars represent ±1σ deviation obtained by propagation of ±1σ deviation on the force constant. (c) modelled $\delta^{34}S$ difference between the BSE and chondrites ($\Delta^{34}S_{BSE\text{-}chondrites}$) as a function of remaining S fraction (f) in the BSE after core formation. Equilibrium and Rayleigh distillation models are considered as two endmember models. In the equilibrium model, $\Delta^{34}S_{BSE\text{-}chondrites}=(1-f)*\Delta^{34}S_{silicate\text{-}metal}$; in the Rayleigh distillation model, $\delta^{34}S_{BSE\text{-}chondrites}=-\Delta^{34}S_{silicate\text{-}metal}*\ln(f)$. From (a) and (b), $\Delta^{34}S_{silicate\text{-}metal}$ is $< +0.02$‰ at > 3500 K and 0-60 GPa, which leads to a positive shift of 0.02-0.1‰ in $\delta^{34}S_{BSE}$.

Figure 3. Sulfur isotope fractionation caused by volatile loss during planetesimal

evaporation and the Moon-forming impact. (a) the modelled $\Delta^{34}S_{\text{Earth-chondrites}}$ as a function of the S fraction remaining after S evaporation from molten planetesimals under different temperatures (1300 K, 1400 K, and 1500 K). At a total gas pressure of about 10^{-4} bar[12], the net evaporation fractionation factor of S isotopes would be equal to the equilibrium vapor-melt S isotope fractionation factor ($\Delta^{34}S^{eq}_{\text{vapor-melt}}$), and $\Delta^{34}S_{\text{Earth-chondrites}}=\Delta^{34}S^{eq}_{\text{vapor-melt}}*\ln f$, where f is the S fraction remaining. The β factor of vapor phase is estimated based on the fractions of major S species in the vapor phase and their <*F*>, and $\Delta^{34}S^{eq}_{\text{vapor-melt}}=10^{3}\ln\beta_{\text{vapor}}-10^{3}\ln\beta_{\text{melt}}$. (b) the modelled $\Delta^{34}S_{\text{Moon-Earth}}$ as a function of the S fraction remaining after vapor loss (f) and vapor saturation degree (D). The loss of abundant S as atomic gas during the Moon-forming impact can result in a large $\Delta^{34}S_{\text{Moon-Earth}}$. Following a Rayleigh distillation model, $\Delta^{34}S_{\text{Moon-Earth}}=\Delta^{34}S_{\text{vapor-melt}}*\ln f$. $\Delta^{34}S_{\text{vapor-melt}}$ ranges from $\Delta^{34}S^{kin}$ (=[(32/34)$^{1/2}$-1]*1000=-29.8‰) to $\Delta^{34}S^{eq}_{\text{vapor-melt}}$ (=-113000/T^{2}, T is temperature in Kelvin), depending on the vapor saturation degree ($\Delta^{34}S_{\text{vapor-melt}}=\Delta^{34}S^{eq}+(1-D)*\Delta^{34}S^{kin}$)[40]. The S loss fraction that is required to explain the observed $\Delta^{34}S_{\text{Moon-Earth}}$ (+1.98±0.50‰, dash and solid blue lines) depends on the vapor saturation degree.

Figure 4. Schematic diagram of sulfur isotopic behaviors during evaporation on small precursor bodies or during the Moon-forming impact. A: partial melting and S vaporization on molten planetesimals mainly as H_2S under vapor-saturated conditions in the presence of nebular H_2 with a pressure of 10^{-4} bar[12]. This process would cause the enrichment of ^{32}S in proto-Earth and about 90% loss of S could explain the $\Delta^{34}S_{\text{Earth-chondrites}}$. Followed by core formation[7,8], the S abundance of the BSE[38] can be reproduced without the need of the accretion of CI-like materials. **B:** the growing molten Moon condensed from the vapor of BSE composition at locales beyond the Roche limit under high temperature, in which a large amount of S was lost under vapor-undersaturated conditions (a vapor saturation degree of 0.941-0.977).

Data availability. The data that support the findings of this study is available in supplementary information and any additional data can be requested by e-mailing the corresponding authors.

Code availability. The Vienna Ab Initio Simulation Package is a proprietary software available for purchase at https://www.vasp.at/.

References

1. Dauphas, N. The isotopic nature of the Earth's accreting material through time. *Nature* **541**, 521–524 (2017).
2. Wood, B. J., Walter, M. J. & Wade, J. Accretion of the Earth and segregation of its core. *Nature* **441**, 825–833 (2006).
3. Schonbachler, M., Carlson, R. W., Horan, M. F., Mock, T. D. & Hauri, E. H. Heterogeneous Accretion and the Moderately Volatile Element Budget of Earth. *Science (80-.).* **328**, 884–887 (2010).
4. Kleine, T. *et al.* Hf–W chronology of the accretion and early evolution of asteroids and terrestrial planets. *Geochim. Cosmochim. Acta* **73**, 5150–5188 (2009).
5. Norris, C. A. & Wood, B. J. Earth's volatile contents established by melting and vaporization. *Nature* **549**, 507–510 (2017).
6. Hin, R. C. *et al.* Magnesium isotope evidence that accretional vapour loss shapes planetary compositions. *Nature* **549**, 511–527 (2017).
7. Rose-Weston, L., Brenan, J. M., Fei, Y., Secco, R. A. & Frost, D. J. Effect of pressure, temperature, and oxygen fugacity on the metal-silicate partitioning of Te, Se, and S: Implications for earth differentiation. *Geochim. Cosmochim. Acta* **73**, 4598–4615 (2009).
8. Boujibar, A. *et al.* Metal-silicate partitioning of sulphur, new experimental and thermodynamic constraints on planetary accretion. *Earth Planet. Sci. Lett.* **391**, 42–54 (2014).
9. Suer, T.-A., Siebert, J., Remusat, L., Menguy, N. & Fiquet, G. A sulfur-poor terrestrial core inferred from metal–silicate partitioning experiments. *Earth Planet. Sci. Lett.* **469**, 84–97 (2017).
10. O'Neill, H. S. . The origin of the moon and the early history of the earth—A chemical model. Part 1: The moon. *Geochim. Cosmochim. Acta* **55**, 1135–1157 (1991).
11. Braukmüller, N., Wombacher, F., Funk, C. & Münker, C. Earth's volatile element depletion pattern inherited from a carbonaceous chondrite-like source. *Nat. Geosci.* **12**, 564–568 (2019).
12. Lodders, K. Solar System Abundances and Condensation Temperatures of the Elements. *Astrophys. J.* **591**, 1220–1247 (2003).
13. Wang, Z. & Becker, H. Ratios of S, Se and Te in the silicate Earth require a volatile-rich late veneer. *Nature* **499**, 328–331 (2013).
14. Yierpan, A., König, S., Labidi, J. & Schoenberg, R. Selenium isotope and S-Se-Te elemental systematics along the Pacific-Antarctic ridge: Role of mantle processes. *Geochim. Cosmochim. Acta* **249**, 199–224 (2019).
15. Labidi, J., Cartigny, P. & Moreira, M. Non-chondritic sulphur isotope composition of the terrestrial mantle. *Nature* **501**, 208–211 (2013).
16. Labidi, J., Cartigny, P., Hamelin, C., Moreira, M. & Dosso, L. Sulfur isotope budget (32S,33S,34S and36S) in Pacific-Antarctic ridge basalts: A record of

mantle source heterogeneity and hydrothermal sulfide assimilation. *Geochim. Cosmochim. Acta* **133**, 47–67 (2014).

17. Gao, X. & Thiemens, M. H. Isotopic composition and concentration of sulfur in carbonaceous chondrites. *Geochim. Cosmochim. Acta* **57**, 3159–3169 (1993).
18. Gao, X. & Thiemens, M. H. Variations of the isotopic composition of sulfur in enstatite and ordinary chondrites. *Geochim. Cosmochim. Acta* **57**, 3171–3176 (1993).
19. Labidi, J., Farquhar, J., Alexander, C. M. O. D., Eldridge, D. L. & Oduro, H. Mass independent sulfur isotope signatures in CMs: Implications for sulfur chemistry in the early solar system. *Geochim. Cosmochim. Acta* **196**, 326–350 (2017).
20. Labidi, J. *et al.* Experimentally determined sulfur isotope fractionation between metal and silicate and implications for planetary differentiation. *Geochim. Cosmochim. Acta* **175**, 181–194 (2016).
21. Fischer, R. A. *et al.* High pressure metal–silicate partitioning of Ni, Co, V, Cr, Si, and O. *Geochim. Cosmochim. Acta* **167**, 177–194 (2015).
22. Sanloup, C. *et al.* Structural change in molten basalt at deep mantle conditions. *Nature* **503**, 104–107 (2013).
23. Sun, N., Stixrude, L., Koker, N. de & Karki, B. B. First principles molecular dynamics simulations of diopside (CaMgSi2O6) liquid to high pressure. *Geochim. Cosmochim. Acta* **75**, 3792–3802 (2011).
24. De Koker, N. Structure, thermodynamics, and diffusion in CaAl2Si2O8 liquid from first-principles molecular dynamics. *Geochim. Cosmochim. Acta* **74**, 5657–5671 (2010).
25. McEwing, C. ., Thode, H. . & Rees, C. . Sulphur isotope effects in the dissociation and evaporation of troilite: A possible mechanism for 34S enrichment in lunar soils. *Geochim. Cosmochim. Acta* **44**, 565–571 (1980).
26. Young, E. D. *et al.* Near-equilibrium isotope fractionation during planetesimal evaporation. *Icarus* **323**, 1–15 (2019).
27. Bigeleisen, J. & Mayer, M. G. Calculation of Equilibrium Constants for Isotopic Exchange Reactions. *J. Chem. Phys.* **15**, 261 (1947).
28. Nash, W. M., Smythe, D. J. & Wood, B. J. Compositional and temperature effects on sulfur speciation and solubility in silicate melts. *Earth Planet. Sci. Lett.* **507**, 187–198 (2019).
29. Jugo, P. J., Wilke, M. & Botcharnikov, R. E. Sulfur K-edge XANES analysis of natural and synthetic basaltic glasses: Implications for S speciation and S content as function of oxygen fugacity. *Geochim. Cosmochim. Acta* **74**, 5926–5938 (2010).
30. Wadhwa, M. Redox Conditions on Small Bodies, the Moon and Mars. *Rev. Mineral. Geochemistry* **68**, 493–510 (2008).
31. McCammon, C. GEOCHEMISTRY: The Paradox of Mantle Redox. *Science*

(80-.). **308**, 807–808 (2005).

32. Rubie, D. C., Nimmo, F. & Melosh, H. J. Formation of the Earth's Core. in *Treatise on Geophysics* 43–79 (Elsevier, 2015). doi:10.1016/B978-0-444-53802-4.00154-8.
33. Righter, K. Prediction of metal-silicate partition coefficients for siderophile elements: An update and assessment of PT conditions for metal-silicate equilibrium during accretion of the Earth. *Earth Planet. Sci. Lett.* **304**, 158–167 (2011).
34. Rubie, D. C. *et al.* Accretion and differentiation of the terrestrial planets with implications for the compositions of early-formed Solar System bodies and accretion of water. *Icarus* **248**, 89–108 (2015).
35. Grewal, D. S., Dasgupta, R., Sun, C., Tsuno, K. & Costin, G. Delivery of carbon, nitrogen, and sulfur to the silicate Earth by a giant impact. *Sci. Adv.* **5**, eaau3669 (2019).
36. Varas-Reus, M. I., König, S., Yierpan, A., Lorand, J.-P. & Schoenberg, R. Selenium isotopes as tracers of a late volatile contribution to Earth from the outer Solar System. *Nat. Geosci.* **12**, 779–782 (2019).
37. Sharp, Z. D. Nebular ingassing as a source of volatiles to the Terrestrial planets. *Chem. Geol.* **448**, 137–150 (2017).
38. McDonough, W. F. & Sun, S. -s. The composition of the Earth. *Chem. Geol.* **120**, 223–253 (1995).
39. Mann, U., Frost, D. J., Rubie, D. C., Becker, H. & Audétat, A. Partitioning of Ru, Rh, Pd, Re, Ir and Pt between liquid metal and silicate at high pressures and high temperatures - Implications for the origin of highly siderophile element concentrations in the Earth's mantle. *Geochim. Cosmochim. Acta* **84**, 593–613 (2012).
40. Nie, N. X. & Dauphas, N. Vapor Drainage in the Protolunar Disk as the Cause for the Depletion in Volatile Elements of the Moon. *Astrophys. J.* **884**, L48 (2019).
41. Wang, K. & Jacobsen, S. B. Potassium isotopic evidence for a high-energy giant impact origin of the Moon. *Nature* **538**, 487–490 (2016).
42. Paniello, R. C., Day, J. M. D. & Moynier, F. Zinc isotopic evidence for the origin of the Moon. *Nature* **490**, 376–379 (2012).
43. Lock, S. J. *et al.* The Origin of the Moon Within a Terrestrial Synestia. *J. Geophys. Res. Planets* **123**, 910–951 (2018).
44. Schaefer, L., Lodders, K. & Fegley, B. VAPORIZATION OF THE EARTH: APPLICATION TO EXOPLANET ATMOSPHERES. *Astrophys. J.* **755**, 41 (2012).
45. Day, J. M. D. Geochemical constraints on residual metal and sulfide in the sources of lunar mare basalts. *Am. Mineral.* **103**, 1734–1740 (2018).
46. Saal, A. E. & Hauri, E. H. Large sulfur isotope fractionation in lunar volcanic glasses reveals the magmatic differentiation and degassing of the Moon. *Sci.*

Adv. **7**, 1–12 (2021).

47. Wing, B. A. & Farquhar, J. Sulfur isotope homogeneity of lunar mare basalts. *Geochim. Cosmochim. Acta* **170**, 266–280 (2015).
48. Franz, H. B. *et al.* Isotopic links between atmospheric chemistry and the deep sulphur cycle on Mars. *Nature* **508**, 364–368 (2014).
49. Rai, V. K., Jackson, T. L. & Thiemens, M. H. Photochemical mass-independent sulfur isotopes in achondritic meteorites. *Science* **309**, 1062–5 (2005).
50. Wu, N., Farquhar, J., Dottin, J. W. & Magalhães, N. Sulfur isotope signatures of eucrites and diogenites. *Geochim. Cosmochim. Acta* **233**, 1–13 (2018).
51. Defouilloy, C., Cartigny, P., Assayag, N., Moynier, F. & Barrat, J.-A. High-precision sulfur isotope composition of enstatite meteorites and implications of the formation and evolution of their parent bodies. *Geochim. Cosmochim. Acta* **172**, 393–409 (2016).
52. Antonelli, M. A. *et al.* Early inner solar system origin for anomalous sulfur isotopes in differentiated protoplanets. *Proc. Natl. Acad. Sci.* **111**, 17749–17754 (2014).
53. Dottin, J. W., Farquhar, J. & Labidi, J. Multiple sulfur isotopic composition of main group pallasites support genetic links to IIIAB iron meteorites. *Geochim. Cosmochim. Acta* **224**, 276–281 (2018).

Methods

Equilibrium isotope fractionation factor

Bigeleisen–Mayer equation[27] has been widely used to calculate the reduced partition function ratio (β) of element X in phase A, which represents the equilibrium isotope fractionation factor of element X between the phase A and an ideal gas of X atoms. Under the high-temperature approximation, the Bigeleisen–Mayer equation can be expressed as:

$$\beta = 1 + \left(\frac{1}{m} - \frac{1}{m'}\right)\frac{\hbar^2}{24k^2T^2}\left(f_{xx} + f_{yy} + f_{zz}\right) \tag{1}$$

where m and m' refer to the light and heavy isotopes, respectively; f_{xx}, f_{yy}, and f_{zz} are the diagonal elements of the force constant matrix; T is temperature in Kelvin, and $\hbar$ and k are the reduced Planck constant and Boltzmann constant, respectively. Thus, the equilibrium isotope fractionation factor between phase A and B can be derived from:

$$10^3 ln\alpha_{A-B} = 10^3 ln\beta_A - 10^3 ln\beta_B = \left(\frac{1}{m} - \frac{1}{m'}\right)\frac{\hbar^2}{8k^2T^2}\left(< F >_A - < F >_B\right) \tag{2}$$

Here $< F >$ is defined as the average value of diagonal elements of the force constant matrix $(f_{xx} + f_{yy} + f_{zz})/3$. The use of Eq. (2) requires the validity criteria that frequencies related to the element of interest ω_i (cm^{-1}) ≤ 1.39 T (T is the temperature in Kelvin). For the temperature of core formation (> 3000 K), the upper limit of frequencies is > 4200 cm^{-1}, which is higher than any vibrational frequency associated with S atom in secular materials. This method has been also successfully applied to predict the equilibrium barium isotope fractionation between minerals and aqueous solution at low temperature[54] and the nickel isotope fractionation between silicate and metallic melts[55].

First-principles molecular dynamics simulations

Equilibrium sulfur (S) isotope fractionation factors between silicate and metallic melts can be estimated from the <F> difference between these two melts using Eq. (2). Because melts do not have regular structures as solid crystals, we conducted first-principles molecular dynamics (FPMD) simulations based on the density functional theory (DFT) using VASP with the projector-augmented wave (PAW) method[56] to predict the structures of S-bearing silicate and metallic melts. The generalized-gradient approximation (GGA)[57] was adopted for the exchange-correlation functional and the PBE pseudopotentials were used. The energy cutoff for the plane wave was 600 eV. The Brillouin zone summations over the electronic states were performed at gamma point. Here we firstly focus on three different melts, including metallic melt with a chemical formula of $Fe_{97}S_3$ and two silicate melts with chemical formulas of $Mg_{32}Si_{32}O_{95}S$ and $Mg_{32}Si_{32}O_{96}SO_2$. The former silicate melt represents the S-bearing silicate melt under relatively reducing condition and the latter refers to relatively oxidizing condition. The chemical composition of $MgSiO_3$ was chosen for silicate melts because it has similar MgO and SiO_2 contents to primitive chondrites. In order to check the effect of other minor elements on the structural properties obtained for S in silicate and metallic melt, we also conducted FPMD simulations on a pyrolitic composition ($Mg_{41}Ca_2Fe_5Si_{32}Al_4O_{117}S$) and a multicomponent alloy ($Fe_{87}Ni_4Si_{10}O_2C_2S_3$) under relatively reducing condition. All FPMD simulations were performed in the NVT thermodynamic ensemble with a fixed temperature controlled by a Nosé thermostat. The simulations for Fe-bearing systems are spin - polarized, with the spin on each Fe atom being allowed to freely fluctuate at each step. We did not introduce a Hubbard U correction for Fe atoms in our calculations. Caracas et al.[58] checked the behavior of the Fe-bearing melt based on DFT+U and found that a +U correction does not significantly change the calculated results. Cell parameters and volumes of simulated boxes are listed in Supplementary Table 1. The time step was set to be 1 fs and the initial liquid configurations at different volumes were prepared by melting the structures at 6000 K for 20 ps. After that, all simulations were conducted at 3000 K for at least 60 ps. Pressures at different volumes can be derived by averaging the pressure for each time step after the equilibration.

To obtain the force constant of S atom in silicate and metallic melts, large numbers of snapshots were extracted from the FPMD trajectories every 250 steps after equilibration for the single-atom optimization, in which only S atomic positions were relaxed with fixed cubic boxes. Then the force constant matrix of S in each snapshot can be calculated using the small displacement method (see Supplementary Information) and the statistical average on all snapshots is the average force constant of S atom in the melts.

Our results suggest the Si-O distance initially increases from ~ 1.62 Å at 6.28 GPa to ~ 1.67 Å at 66.85 GPa and then maintains at ~ 1.66 Å with further compression (Supplementary Fig. 1 and 2), whereas the Mg-O bond length significantly decreases from 1.97 to 1.88 Å when the pressure increases from 6.28 GPa to 105.03 GPa. Meanwhile, the coordination numbers (CNs) for Si-O and Mg-O pairs increase from ~ 4.1 to 6 and from ~ 4.1 to 7.1 at that pressure range (Supplementary Fig. 1 and 2), respectively. The calculated structural properties agree well with previous experimental measurements[22] and theoretical studies[23,24], ensuring the accuracy and reliability of our calculations. In $Mg_{32}Si_{32}O_{96}SO_2$ melt, the S-O distance (~ 1.5 Å) is much shorter than the S-Mg (> 2.5 Å) and S-Si distances (> 2.8 Å) and the coordination number (CN) for S-O pair is ~3 if the cutoff is 2.0 Å (Extended Data Fig. 1), suggesting that S atom is directly bonded to O atoms as sulfate under relatively oxidizing conditions. In contrast, the S-O distance in $Mg_{32}Si_{32}O_{95}S$ melt (~2.6 Å) is much longer than that in the $Mg_{32}Si_{32}O_{96}SO_2$ melt, while the S-Mg (~2.4 Å) and S-Si distances (~2.05 Å) are much shorter than those in $Mg_{32}Si_{32}O_{96}SO_2$ melt (Extended Data Fig. 2). When the cutoff for the coordination shell is 2.5 Å, the CNs for S-Mg and S-Si pairs are both ~1, suggesting that the S atom is bonded to Si and Mg atoms, which is self-consistent with the valence state of S (S^{2-}). The S atom in $Mg_{41}Ca_2Fe_5Si_{32}Al_4O_{117}S$ melt is preferentially bonded to Fe and Mg atoms (Extended Data Fig. 4), but the S-Fe distance (~ 2.10 Å) is shorter than the S-Mg distance (~ 2.37 Å). The CNs for S-Fe and S-Mg pairs are ~2 and 1, respectively, when the cutoff for the coordination shell is 2.5 Å. In $Fe_{97}S_3$ melt, the S-Fe distance (2.09-2.15 Å) is comparable to the S-Fe distance in

$Mg_{41}Ca_2Fe_5Si_{32}Al_4O_{117}S$ melt and the CNs are 4-5 if the cutoff is 2.4 Å (Extended Data Fig. 3). In $Fe_{87}Ni_4Si_{10}O_2C_2S_3$ melt, the S atom is dominantly bonded to Fe and Ni atoms with a S-Fe/Ni distance of ~2.11 Å (Extended Data Fig. 4), similar to the S-Fe distance in $Fe_{97}S_3$ melt.

The <F> of S in each snapshot and the statistical average are shown in Supplementary Fig. 3-6. Our results show that the <F> difference between silicate and metallic melts is smaller than 25 N/m at < 80 GPa (Extended Data Fig. 5 and Supplementary Table 1) when S^{2-} is the dominant species, suggesting no significant equilibrium S isotope fractionation between these two phases (Fig. 2). The <F> of S in $Mg_{41}Ca_2Fe_5Si_{32}Al_4O_{117}S$ and $Fe_{87}Ni_4Si_{10}O_2C_2S_3$ melts are 291.6 N/m at 46.6 GPa and 253.8 N/m at 41.8 N/m, which are only ~15 N/m higher than the values for $Mg_{32}Si_{32}O_{95}S$ and $Fe_{97}S_3$ systems (Extended Data Fig. 5). This indicates that the presence of other components does not significantly affect the the $10^3\ln\alpha$ between silicate and metallic melts under relatively reducing condition. Previous experimental work argued that Fe metal is preferentially enriched in ^{34}S relative to silicate melt and the fractionation is up to +0.64 ‰ at 1923 K. If this is correct, the <*F*> of S in silicate melt should be at least 290 N/m lower than that the one in metallic melt, which deviates from the direction of our predictions. This is likely because the isotope exchange during experiments had not reached the equilibrium state.

Sulfur species in vapor phases

In order to estimate the equilibrium S isotope fractionation between the vapor phase and silicate melt, we first determined the S species in the vapor phase. We used the GRAINS code[59] to calculate the minimum Gibbs free energy of the system with solar abundance for the elements[12] at specific temperature and $1e^{-4}$ bar. This code considered 33 elements (H, He, C, N, O, Na, Mg, Al, Si, P, S, Cl, K, Ca, Ti, Cr, Mn, Fe, Co, Ni, Cu, Ga, Ge, Mo, Ru, Pd, Hf, W, Re, Os, Ir, Pt, Au). The code considers 242 gas species and 520 condensed (liquid or solid) species freely and outputs all the species when the system achieves chemical equilibrium through Gibbs free energy minimization. We used the solar abundances for the elements to calculate the equilibrium gas phases because the solar nebular would not have completely dissipated during planetesimal evaporation in the first several million years[37]. The evaporation of planetesimals investigated here requires the presence of nebular H_2 under a total pressure of $1e^{-4}$ bar. The results of all S species at 1000-1600 K and $1e^{-4}$ bar are listed in Supplementary Table 2. The important species for S in the vapor includes H_2S (g), HS (g), SiS (g), and S_2 (g), among which the fraction of H_2S is the largest at 1000-1500 K. To check the effect of H concentration on the S species in the vapor phase, we also conducted thermodynamic calculations using GRAINS with solar elemental abundances but with H concentration decreased by one and four orders of magnitude, conditions that are more oxidizing than the solar nebular. The results show that S in the vapor phase mainly occurs as H_2S and/or HS at 1000-1500 K when H concentration is decreased by 90%, while SO, SO_2, and S_2 are the main S species when only 0.01% H is retained (Extended Data Fig. 7). On the basis of these results, we conducted first-principles calculations for these S species in the vapor phase. For each S species, we put a molecule in a cubic box (20 Å×20 Å×20 Å) and relaxed the atomic positions. The <F> of S can be estimated using the small displacement method (Supplementary Table 1). We checked the effect of box size and found that the results will not change with the size when the cell parameter is larger than 20 Å. The atomic S gas has a <F> of 0 N/m and the β factor is 0, because there is no atomic bonding in this system. Thus, the <F> of S in the vapor with the presence of nebular H_2 can be calculated based on the fractions of each species (Supplementary Table 2).

Isotope fractionation during evaporation and condensation

Young et al.[26] investigated the nature of evaporation process and how evaporation and condensation fractionate isotopes using numerical simulations. Following that work, the S isotope fractionation during evaporation and condensation ($\Delta^{34}S_{\text{vapor-melt}}$)

can be approximately expressed as:

$$\Delta^{34}S_{vapor\text{-}melt}=\Delta^{34}S^{eq}+(1\text{-}D)*\Delta^{34}S^{kin} \quad (3)$$

where $\Delta^{34}S^{eq}$ is the equilibrium S isotope fractionation between vapor phase and melt, $\Delta^{34}S^{kin}$ is the kinetic S isotope fractionation, and D is the degree vapor saturation ($D=P/P_{sat}$, P is the pressure of the evaporating species at the surface of the melt and P_{sat} is the saturation vapor pressure). $\Delta^{34}S^{kin}$ can be estimated from: $\Delta^{34}S^{kin} = 1000*[(m_{S32}/m_{S34})^{1/2} - 1]$, where is the atomic or molecular mass of the vapor species. This simplified approach gives the instantaneous isotopic fractionation between vapor and melt.

The effect of planetesimal evaporation on the $\delta^{34}S$ of proto-Earth and other differentiated bodies depends on the degree vapor saturation and S species in the vapor phase that are a function of oxygen fugacity and temperature. If D is lower than 100%, the net evaporation fractionation factor of S isotopes ($\Delta^{34}S_{vapor\text{-}melt}$) would be affected by the large negative kinetic fractionation, and the final $\Delta^{34}S_{vapor\text{-}melt}$ could be positive, zero, or negative even when the S evaporates mainly as H_2S from planetesimals. On the other hand, when D is 100%, $\Delta^{34}S_{vapor\text{-}melt}$ is controlled by the S species in the vapor phase. The evaporation of atomic S will enrich the melt in heavy S isotopes, whereas H_2S evaporation will enrich the melt in light S isotopes.

Differentiated planetesimals may have undergone S evaporation under a range of conditions, which may show different effects on their $\delta^{34}S$ values. When planetesimals undergo evaporation in the presence of nebular H_2 under a total pressure of about 10^{-4} bar, numerical simulations[26] show that the vapor saturation degree will be approximately 100%, and the net isotope fractionation is equal to the equilibrium isotope fractionation between vapor and melt. The evaporation of planetesimal melts in the presence of nebular H_2 can also explain the Mg and Si isotopic and elemental compositions of the bulk Earth[26]. The observed bulk Earth S isotope signature and abundance can be reproduced by the evaporative loss of ~90% S, mainly as H_2S, from molten planetesimals in a H_2 atmosphere. For Mars, previous studies reported that most sulfides in shergotiites have negative $\delta^{34}S$ values, indicating that the Martian mantle is also likely to have a negative $\delta^{34}S$ value. The average S concentration for all shergotiites[48] is about four times the S abundance in the BSE. As such, the evaporative loss of S (~60%) would be significantly lower than the estimate for Earth and the effect of evaporation on the $\delta^{34}S$ value ($\Delta^{34}S_{\text{Mars-chondrites}}=\Delta^{34}S^{eq}_{\text{vapor-melt}}*\ln f$, where f is the S fraction remaining) would be smaller than that for Earth. So overall, the literature data of sulfides in shergotiites primary supports our conclusions.

References

54. Wang, W., Wu, Z. & Huang, F. Equilibrium barium isotope fractionation between minerals and aqueous solution from first-principles calculations. *Geochim. Cosmochim. Acta* **292**, 64–77 (2021).
55. Wang, S.-J. *et al.* Nickel isotopic evidence for late-stage accretion of Mercury-like differentiated planetary embryos. *Nat. Commun.* **12**, 294 (2021).
56. Blöchl, P. E. Projector augmented-wave method. *Phys. Rev. B* **50**, 17953–17979 (1994).
57. Perdew, J. P., Burke, K. & Ernzerhof, M. Generalized Gradient Approximation Made Simple. *Phys. Rev. Lett.* **77**, 3865–3868 (1996).
58. Caracas, R., Hirose, K., Nomura, R. & Ballmer, M. D. Melt–crystal density crossover in a deep magma ocean. *Earth Planet. Sci. Lett.* **516**, 202–211 (2019).
59. Petaev, M. I. The GRAINS thermodynamic and kinetic code for modeling nebular condensation. *Calphad* **33**, 317–327 (2009).

Sulfur isotopic signature of Earth established by planetesimal volatile evaporation

Wenzhong Wang[1,2,3,*], Chun-Hui Li[4,5,*], John P. Brodholt[2,6], Shichun Huang[7], Michael J. Walter[3], Min Li[8], Zhongqing Wu[1,9,10], Fang Huang[5,9], Shui-Jiong Wang[11]

[1]Laboratory of Seismology and Physics of Earth's Interior, School of Earth and Space Sciences, University of Science and Technology of China, Hefei, Anhui 230026, China

[2]Department of Earth Sciences, University College London, London WC1E 6BT, United Kingdom

[3]Earth and Planets Laboratory, Carnegie Institution for Science, Washington, DC 20015, USA

[4]International Center for Planetary Science, College of Geosciences, Chengdu University of Technology, Chengdu 610059, China

[5]CAS Key Laboratory of Crust-Mantle Materials and Environments, School of Earth and Space Sciences, University of Science and Technology of China, Hefei, Anhui 230026, China

[6]Centre for Earth Evolution and Dynamics, University of Oslo, Oslo, Norway

[7]Department of Geoscience, University of Nevada, Las Vegas, United States

[8]Department of Physics and Astronomy, University of Nevada, Las Vegas

[9]CAS Center for Excellence in Comparative Planetology, USTC, Hefei, Anhui 230026, China

[10]National Geophysical Observatory at Mengcheng, USTC, Hefei, China

[11]State Key Laboratory of Geological Processes and Mineral Resources, China University of Geosciences, Beijing, China.

[*]Correspondence and requests for materials should be addressed to W.W. (wenzhong.wang@ucl.ac.uk) and C.-H.L. (lichunhui@cdut.edu.cn).

Abstract

How and when Earth's volatile content was established is controversial with several mechanisms postulated, including planetesimal evaporation, core formation, and the late delivery of undifferentiated chondrite-like materials. The isotopes of volatile elements such as sulfur can be fractionated during planetary accretion and differentiation, and thus are potential tracers of these processes. Using first-principles calculations, we examine sulfur isotope fractionation during core formation and planetesimal evaporation. We find no measurable sulfur isotope fractionation between silicate and metallic melts at core-forming conditions, indicating that the observed light sulfur isotope composition of the bulk silicate Earth relative to chondrites cannot be explained by metal-silicate fractionation. Our thermodynamic calculations show that sulfur evaporates mostly as H_2S during planetesimal evaporation when nebular H_2 is present. The observed bulk Earth sulfur isotope signature and abundance can be reproduced by the evaporative loss of ~90% sulfur mainly as H_2S from molten planetesimals before nebular H_2 is dissipated. The heavy sulfur isotope composition of the Moon relative to the Earth is consistent with evaporative sulfur loss under 94-98% saturation condition during the Moon-forming giant impact. In summary, volatile evaporation from molten planetesimals prior to Earth's formation likely played a key role in establishing Earth's volatile element content.

Understanding the accretion history of Earth's volatile elements, such as sulfur (S), carbon (C), hydrogen (H) and nitrogen (N), is of profound importance for understanding planetary formation, evolution, and habitability. Earth formed from protoplanetary embryos with chemical compositions assumed to be similar to undifferentiated chondrites[1]. Compared with the solar composition and primitive chondrites, the bulk silicate Earth (BSE) has a similar refractory lithophile element abundance pattern but is strongly depleted in volatile elements[2]. Different interpretations have been proposed to explain this strong volatile element depletion. For instance, the depletion pattern could be explained qualitatively by the late accretion of 10-20% of a volatile-rich body to a volatile-depleted proto-Earth[3]. Partial melting and vaporization on bodies heated by the decay of short-lived nuclei[4], such as ^{26}Al, may have caused extensive volatile loss in the protoplanetary embryos that formed Earth[5,6]. Depletion of some siderophile (iron-loving) elements, such as S, may also be associated with core-mantle differentiation[7–9] and/or the Hadean sulfide segregation into the core[10]. However, a recent study[11] argued that the volatile depletion in the BSE was inherited from a carbonaceous chondrite-like source, suggesting that exotic addition of materials or vaporization from Earth's precursors are not strictly required.

The abundance of volatiles and their isotopic compositions are commonly used to distinguish between different mechanisms for establishing a volatile depleted mantle. Sulfur, selenium (Se), and tellurium (Te) are highly siderophile elements with similar and relatively low 50% condensation temperatures in a solar nebula composition gas[12]. Measurements of S, Se, and Te abundances in mantle peridotites suggest that a volatile-rich late veneer of carbonaceous-chondrite-like material is required to explain the relative ratios of S, Se and Te in the BSE[13], but it is debated whether peridotites preserve primitive mantle signatures[14]. The BSE has an average stable S isotope composition (expressed as $\delta^{34}S = [(^{34}S/^{32}S)_{sample}/(^{34}S/^{32}S)_{CDT} - 1] \times 1000$ ‰ and CDT is Canyon Diablo Troilite) of -1.40 ± 0.50‰ (1SD)[15,16], which is significantly lower than the average chondritic values[17–19] (Fig. 1). Labidi et al.[15,16] argued that core-mantle differentiation[7,8], rather than a late veneer, was responsible for the sub-chondritic $\delta^{34}S$ of the BSE. Equilibrium S isotope fractionation factors at core-forming conditions are required to test this hypothesis, however, to date such data are not well constrained. Published experiments[20] on S isotope fractionation between metal and silicate melt have been performed only at < 2 GPa and < 2000 K, whereas the pressure and temperature (*P*-*T*) for Earth's core formation are expected to be much higher[21]. Both experimental and theoretical studies[22–24] demonstrate that the structure of silicate melts changes dramatically with pressure, indicating that metal-silicate S isotopic fractionation measured at low pressure cannot be directly applied to high-pressure core formation[20].

As a volatile element, S would have undergone significant vaporization during Earth's accretion like other moderately volatile elements[5] such as Bi, Sn, Pb, and Zn. Previous studies have investigated S isotope fractionation during evaporation from troilite[25], and Mg and Si isotope fractionation during planetesimal evaporation[6,26], but the effect of evaporation on S isotopes from planetesimals is unexplored. Whether the sub-chondritic $\delta^{34}S$ of the BSE is related to S loss during early vaporization from Earth's precursor bodies fundamentally impacts our understanding of the volatile depletion in the BSE.

Structural properties of sulfur in melts

Here we present first-principles calculations that constrain the equilibrium S isotope fractionation between silicate and metallic melts, and between the vapor phase and silicate melt. We first conducted first-principles molecular dynamics (FPMD) simulations based on density functional theory (DFT) (see Methods) to obtain the structures of S-bearing silicate and metallic melts at 4-105 GPa and 3000 K. The structural information of S shows a large difference under relatively reducing and oxidizing conditions. Under relatively oxidizing conditions ($Mg_{32}Si_{32}O_{96}SO_2$), S is directly bonded to O to form sulfate with a short S-O distance of ~ 1.5 Å (Extended Data Fig. 1). In contrast, S is bonded to Fe, Mg and/or Si in $Mg_{32}Si_{32}O_{95}S$ and $Mg_{41}Ca_2Fe_5Si_{32}Al_4O_{117}S$ melts (Extended Data Fig. 2), which correspond to relatively reducing conditions. In $Fe_{97}S_3$ and $Fe_{87}Ni_4Si_{10}O_2C_2S_3$ melts, S is dominantly bonded to Fe and/or Ni with a S-Fe/Ni distance of ~2.1 Å (Extended Data Fig. 3 and 4).

The average force constants <*F*> of S in silicate and metallic melts (Extended Data Fig. 5 and Supplementary Table 1) were estimated using the small displacement method based on the harmonic approximation (see Methods and supporting materials).

The <*F*> values of S are dominated by structural properties such as bond lengths. For instance, the <*F*> of S in the $Mg_{32}Si_{32}O_{96}SO_2$ melt is much larger than those in $Mg_{32}Si_{32}O_{95}S$, $Mg_{41}Ca_2Fe_5Si_{32}Al_4O_{117}S$, $Fe_{87}Ni_4Si_{10}O_2C_2S_3$, and $Fe_{97}S_3$ melts, which can be explained by the much shorter S-O distance in $Mg_{32}Si_{32}O_{96}SO_2$ than the S-Mg/Fe/Si/Ni distances in melts under relatively reducing conditions. In contrast, the <*F*> of S in reducing silicate melts ($Mg_{32}Si_{32}O_{95}S$ and $Fe_{87}Ni_4Si_{10}O_2C_2S_3$) are slightly larger than those in metallic melts ($Fe_{97}S_3$ and $Fe_{87}Ni_4Si_{10}O_2C_2S_3$), although this difference becomes somewhat greater at > 80 GPa. Both silicate and metallic melts become substantially more packed with increasing compression and hence, their S force constants increase significantly with pressure. Compared with $Mg_{32}Si_{32}O_{95}S$ and $Fe_{97}S_3$ melts, the <*F*> of S in $Mg_{41}Ca_2Fe_5Si_{32}Al_4O_{117}S$ and $Fe_{87}Ni_4Si_{10}O_2C_2S_3$ melts only increase by ~15 N/m (Extended Data Fig. 5).

Sulfur isotope fractionation during core formation

Using the high-temperature approximation of the Bigeleisen–Mayer equation[27], we calculated the reduced partition function ratio ($10^3\ln\beta$ or β factor) of $^{34}S/^{32}S$ from the <*F*> (Extended Data Fig. 6) and the equilibrium S isotope fractionation factors ($10^3\ln\alpha$) between silicate and metallic melts at different pressures (Fig. 2). Our results demonstrate that the oxidizing $Mg_{32}Si_{32}O_{96}SO_2$ silicate melt is enriched in ^{34}S relative to metallic melts, but there is no measurable equilibrium S isotope fractionation between the reducing silicate and metallic melts within the range of < 80 GPa. The substantial changes in melt structural properties under compression only mildly affect the $10^3\ln\alpha$ between silicate and metallic melts. At 3000 K and 0-90 GPa, the $10^3\ln\alpha$ between the reducing silicate and metallic melts is smaller than 0.05‰, while the value between $Mg_{32}Si_{32}O_{96}SO_2$ and $Fe_{97}S_3/Fe_{87}Ni_4Si_{10}O_2C_2S_3$ is 0.35±0.02 ‰. Thus, the S isotope fractionation between the mantle and core is dominated by the S speciation in the silicate melt.

The speciation of S in silicate melt is strongly controlled by the oxygen fugacity

(fO_2)[28,29]. At log fO_2 < FMQ-1 (1 log unit lower than the Fayalite–Magnetite–Quartz buffer), S^{2-} is the dominant species; at log fO_2 > FMQ+2, S occurs as S^{6+}, whereas at FMQ-1 < log fO_2 < FMQ+2, S^{2-} and S^{6+} coexist, and S^{6+} content increases sharply with log fO_2. Under the redox conditions of core formation for Earth, Mars, and Moon (< FMQ-4)[30,31], S^{2-} should be the dominant species in silicate melt, and our results show no measurable S isotope fractionation between silicate and metallic melts is predicted (Fig. 2), and this conclusion is independent of the pressure of core formation[2,32]. Calculations using two endmember models (equilibrium and Rayleigh distillation)[2,33,34] show that core-mantle differentiation can only cause a very small positive shift of +0.02-0.1‰ in $\delta^{34}S$ of the silicate mantle (Fig. 2c), which cannot explain the negative $\delta^{34}S$ of the BSE relative to chondrites (Fig. 1).

Mechanisms for sulfur isotope signatures in Earth and Moon

In addition to ruling out core formation as the cause of the negative $\delta^{34}S$ of the BSE, the very small fractionation of S isotopes caused by core formation means that metallic cores have similar S isotopic ratios to their silicate mantles. Consequently, the measured BSE isotopic composition[15] of -1.40 ± 0.50‰ should be representative of the bulk Earth. Such a negative $\delta^{34}S_{Earth}$ cannot be explained by late delivery of S to the BSE[11,35,36] because most late-veneer materials have heavier $\delta^{34}S$ than the Earth (Fig. 1). Although the negative $\delta^{34}S$ of CM chondrites could be as low as -1.11± 0.30 ‰, most CM chondrites are characterized by a non-zero $\Delta^{33}S$ (from -0.005 ± 0.02 ‰ to 0.213 ± 0.02 ‰; $\Delta^{33}S = 1000 \times [\delta^{33}S - [(\delta^{34}S + 1)^{0.515} - 1]]$ ‰), which is inconsistent with the zero $\Delta^{33}S$ measured in terrestrial MORB (0.005 ± 0.008 ‰)[19]. The average $\Delta^{33}S$ and $\delta^{34}S$ values of CM chondrites[19] are 0.021 ± 0.068 ‰ and -0.08 ± 0.44‰, respectively, which could produce zero $\Delta^{33}S$ but cannot reproduce the $\delta^{34}S_{Earth}$ value. We therefore now consider whether this sub-chondritic $\delta^{34}S_{Earth}$ may be associated with volatile loss during Earth's accretion.

Small precursor bodies with heat sources such as radiogenic ^{26}Al[4] would have undergone partial melting and vaporization, in which gravitational escape of volatiles is possible if these precursor bodies have relatively small radii (< 1000 km)[26]. Our thermodynamic calculations (see Methods) show that S mainly occurs as H_2S in the vapor phase (Supplementary Table 2) in the presence of nebular H_2 with a total pressure of about 10^{-4} bar[12,37]. Under such conditions, the net fractionation as a consequence of planetesimal evaporation would be equal to the equilibrium isotope fractionation between vapor phase and melt[26]. This kind of planetesimal evaporation can explain the concentrations of Mg and Si and their isotopic signatures of the bulk Earth[26]. Combining the fractions of each major S species with their <*F*> (Supplementary Table 1), we estimated the equilibrium vapor-melt S isotope fractionation ($\Delta^{34}S^{eq}_{\text{vapor-melt}}$) to be ~+0.45‰ at 1400 K (Extended Data Fig. 7). Therefore, S evaporation from planetesimal melts would enrich the melt phase with light S isotopes. About 90% loss of S can explain the $\delta^{34}S$ difference between the bulk Earth and chondrites (Fig. 3). This S evaporation process would leave a bulk Earth accreted from enstatite-chondritic materials (3.3-5.8 wt% S, Wang and Becker[13]) with a S concentration of 3300-5800 ppm. Such an initial S concentration can reproduce the S abundance of the BSE[38] after S sequestration into the core[7,9] without a contribution from a late veneer.

While our model does not require a late veneer, a late delivery of S is still allowed if the amount of S loss during evaporation is greater than 90%. In this case, the proto-Earth would have an even lower $\delta^{34}S$ that would then be increased by the late-veneer addition with a chondrite-like heavier $\delta^{34}S$. The more S is evaporated, the more S is required to be added by a late veneer to match the S abundance in the BSE. However, the $\delta^{34}S$ in the BSE will be close to those of chondrites if the amount of S added by the late veneer is too high, and so to reproduce the S abundance and $\delta^{34}S$ value of the BSE, the amount of S added by a late veneer to the BSE should not exceed ~30% of the present-day BSE's S budget. As such, if the late veneer is characterized by chondrite-like materials with 1.0 wt% S, the mass of late-veneer materials should not exceed 0.4% of Earth's mass, consistent with estimates based on abundances of highly siderophile elements[39].

We can also explain the large $\Delta^{34}S_{\text{Moon-Earth}}$ with the loss of volatile elements during the Moon-forming giant impact (Fig. 3). It was suggested that evaporation of moderately volatile elements under a vapor saturation of ~99% can explain the enrichment of their heavy isotopes in the lunar mantle relative to the BSE[40–42]. A high-energy, high-angular-momentum model[43] suggests that the Moon condensed from a vapor of BSE composition at distances beyond the Roche limit under high temperature (~ 3700 K), Under such conditions, S evaporates as multiple species[44], including S, SO, and SO_2. Because of the high temperature, the $\Delta^{34}S^{eq}_{\text{vapor-melt}}$, which is derived from the $<F>$ differences between all possible S species and silicate melt (Extended Data Fig. 11), is only -0.08–0.2‰. Consequently, the $\Delta^{34}S_{\text{vapor-melt}}$ is controlled by the kinetic S isotope fractionation during free evaporation ($\Delta^{34}S^{kin} = [(32/34)^{1/2} - 1]*1000 = -29.8‰$) and the vapor saturation degree (see Methods). If the S concentration ratio between the primitive lunar mantle[45] and the BSE[38] is used to estimate the fraction of S loss, the $\Delta^{34}S_{\text{vapor-melt}}$ required to explain the $\Delta^{34}S_{\text{Moon-Earth}}$ ranges from -0.64‰ to -1.65‰, corresponding to a vapor saturation degree of 0.941-0.977 (Fig. 3), which is similar to that constrained by the isotopic data of several moderately volatile elements (0.989 ± 0.002)[40]. The small difference may be related to the uncertainties in the estimated lunar $\delta^{34}S$, since S isotopes can be fractionated by magmatic events that complicates the estimation of lunar $\delta^{34}S$[46]. Overall, S evaporation during the Moon-forming event can provide a first-order explanation for the enrichment of heavy S isotopes in the Moon.

In conclusion, we show that core formation does not significantly fractionate S isotopes, and the bulk Earth is enriched in light S isotopes relative to chondrites and the Moon. Evaporative loss of 90% S or greater from planetesimals with H_2S as the major evaporative species in the presence of nebular H_2 with a pressure of about 10^{-4} bar can reproduce the sub-chondritic $\delta^{34}S_{\text{Earth}}$ and the S concentration of the BSE. The large $\Delta^{34}S_{\text{Moon-Earth}}$ can also be explained by S evaporation under vapor-unsaturated conditions (94-98%) during the Moon-forming event (Fig. 4). This work strongly supports the profound role of a melt-vapor reaction[5,6] in establishing Earth's volatile element depletion pattern[2].

Corresponding Author. Wenzhong Wang (wenzhong.wang@ucl.ac.uk; wwang10@carnegiescience.edu) and Chun-Hui Li (lichunhui@cdut.edu.cn).

Acknowledgements: This work is supported by the Strategic Priority Research Program (B) of the Chinese Academy of Sciences (XDB41000000), Natural Science Foundation of China (41925017 and 41721002). W. W. acknowledges support from the UCL-Carnegie Postdoctoral Scholarship. S.H. and M.L. acknowledge support from NSF AST-1910955. Part of calculations were conducted at the Supercomputing Center of the University of Science and Technology of China.

Author contributions: W.W. and C.-H.L. conceived and designed this project. W.W. performed the theoretical calculations. S.H. and M.L. did the GRAINS calculations. W.W. wrote the manuscript with the help of C.-H.L. and all authors contributed to the discussion of the results and revision of the manuscript.

Competing interests. The authors declare no competing interests.

Figure captions

Figure 1. Sulfur isotope compositions ($\delta^{34}S$) of planetary materials. The $\delta^{34}S$ of the BSE is defined by terrestrial mid-ocean ridge basalts[15,16], while the $\delta^{34}S$ of the silicate Moon is defined by mare basalts[47]. The $\delta^{34}S$ of sulfides in shergottites are from Franz et al.[48]. The average $\delta^{34}S$ of Vesta is defined by eucrites and diogenites[49,50]. The $\delta^{34}S$ values of carbonaceous (CI, CV, CO and CM), ordinary, and enstatite chondrites are from Gao and Thiemens[17,18], Labidi et al.[19], and Defouilloy et al.[51]. The average $\delta^{34}S$ of carbonaceous chondrites given by Gao and Thiemens[17,18] is +0.49 ± 0.16 ‰. The average of CM from Labidi et al.[19] is -0.08 ± 0.44 ‰; however, most CM samples have non-zero $\Delta^{33}S$ (mass independent sulfur isotope composition, $\Delta^{33}S = 1000 \times [\delta^{33}S - [(\delta^{34}S + 1)^{0.515} - 1]]$ ‰), reflecting the effect of photochemistry[19]. The average of all chondrites (light grey, -0.20 ± 0.20 ‰) is based on samples with Earth-like $\Delta^{33}S$ values[15,16]. The $\delta^{34}S$ values of iron meteorites and pallasites are from Antonelli et al.[52] and Dottin et al.[53], respectively. Error bars represent ±1σ deviation.

Figure 2. Equilibrium sulfur isotope fractionation factors ($10^3 \ln\alpha$ of $^{34}S/^{32}S$) between silicate and metallic melts. (a) temperature dependence of $10^3 \ln\alpha_{\text{silicate-metal}}$ at different pressures (b) pressure dependence of $10^3 \ln\alpha_{\text{silicate-metal}}$ at different temperatures. $Mg_{32}Si_{32}O_{95}S$ and $Mg_{32}Si_{32}O_{96}SO_2$ represent S-bearing silicate melts under relatively reducing and oxidizing conditions, respectively. Error bars represent ±1σ deviation obtained by propagation of ±1σ deviation on the force constant. (c) modelled $\delta^{34}S$ difference between the BSE and chondrites ($\Delta^{34}S_{\text{BSE-chondrites}}$) as a function of remaining S fraction (f) in the BSE after core formation. Equilibrium and Rayleigh distillation models are considered as two endmember models. In the equilibrium model, $\Delta^{34}S_{\text{BSE-chondrites}}=(1-f)*\Delta^{34}S_{\text{silicate-metal}}$; in the Rayleigh distillation model, $\delta^{34}S_{\text{BSE-chondrites}}=-\Delta^{34}S_{\text{silicate-metal}}*\ln(f)$. From (a) and (b), $\Delta^{34}S_{\text{silicate-metal}}$ is < +0.02‰ at > 3500 K and 0-60 GPa, which leads to a positive shift of 0.02-0.1‰ in $\delta^{34}S_{\text{BSE}}$.

Figure 3. Sulfur isotope fractionation caused by volatile loss during planetesimal

evaporation and the Moon-forming impact. (a) the modelled $\Delta^{34}S_{Earth\text{-}chondrites}$ as a function of the S fraction remaining after S evaporation from molten planetesimals under different temperatures (1300 K, 1400 K, and 1500 K). At a total gas pressure of about 10^{-4} bar[12], the net evaporation fractionation factor of S isotopes would be equal to the equilibrium vapor-melt S isotope fractionation factor ($\Delta^{34}S^{eq}_{vapor\text{-}melt}$), and $\Delta^{34}S_{Earth\text{-}chondrites}=\Delta^{34}S^{eq}_{vapor\text{-}melt}*\ln f$, where f is the S fraction remaining. The β factor of vapor phase is estimated based on the fractions of major S species in the vapor phase and their <*F*>, and $\Delta^{34}S^{eq}_{vapor\text{-}melt}=10^3\ln\beta_{vapor}-10^3\ln\beta_{melt}$. (b) the modelled $\Delta^{34}S_{Moon\text{-}Earth}$ as a function of the S fraction remaining after vapor loss (f) and vapor saturation degree (D). The loss of abundant S as atomic gas during the Moon-forming impact can result in a large $\Delta^{34}S_{Moon\text{-}Earth}$. Following a Rayleigh distillation model, $\Delta^{34}S_{Moon\text{-}Earth}=\Delta^{34}S_{vapor\text{-}melt}*\ln f$. $\Delta^{34}S_{vapor\text{-}melt}$ ranges from $\Delta^{34}S^{kin}$ ($=[(32/34)^{1/2}-1]*1000=-29.8‰$) to $\Delta^{34}S^{eq}_{vapor\text{-}melt}$ ($=-113000/T^2$, T is temperature in Kelvin), depending on the vapor saturation degree ($\Delta^{34}S_{vapor\text{-}melt}=\Delta^{34}S^{eq}+(1-D)*\Delta^{34}S^{kin}$)[40]. The S loss fraction that is required to explain the observed $\Delta^{34}S_{Moon\text{-}Earth}$ (+1.98±0.50‰, dash and solid blue lines) depends on the vapor saturation degree.

Figure 4. Schematic diagram of sulfur isotopic behaviors during evaporation on small precursor bodies or during the Moon-forming impact. A: partial melting and S vaporization on molten planetesimals mainly as H_2S under vapor-saturated conditions in the presence of nebular H_2 with a pressure of 10^{-4} bar[12]. This process would cause the enrichment of ^{32}S in proto-Earth and about 90% loss of S could explain the $\Delta^{34}S_{Earth\text{-}chondrites}$. Followed by core formation[7,8], the S abundance of the BSE[38] can be reproduced without the need of the accretion of CI-like materials. **B:** the growing molten Moon condensed from the vapor of BSE composition at locales beyond the Roche limit under high temperature, in which a large amount of S was lost under vapor-undersaturated conditions (a vapor saturation degree of 0.941-0.977).

Data availability. The data that support the findings of this study is available in supplementary information and any additional data can be requested by e-mailing the corresponding authors.

Code availability. The Vienna Ab Initio Simulation Package is a proprietary software available for purchase at https://www.vasp.at/.

References

1. Dauphas, N. The isotopic nature of the Earth's accreting material through time. *Nature* **541**, 521–524 (2017).
2. Wood, B. J., Walter, M. J. & Wade, J. Accretion of the Earth and segregation of its core. *Nature* **441**, 825–833 (2006).
3. Schonbachler, M., Carlson, R. W., Horan, M. F., Mock, T. D. & Hauri, E. H. Heterogeneous Accretion and the Moderately Volatile Element Budget of Earth. *Science (80-.).* **328**, 884–887 (2010).
4. Kleine, T. *et al.* Hf–W chronology of the accretion and early evolution of asteroids and terrestrial planets. *Geochim. Cosmochim. Acta* **73**, 5150–5188 (2009).
5. Norris, C. A. & Wood, B. J. Earth's volatile contents established by melting and vaporization. *Nature* **549**, 507–510 (2017).
6. Hin, R. C. *et al.* Magnesium isotope evidence that accretional vapour loss shapes planetary compositions. *Nature* **549**, 511–527 (2017).
7. Rose-Weston, L., Brenan, J. M., Fei, Y., Secco, R. A. & Frost, D. J. Effect of pressure, temperature, and oxygen fugacity on the metal-silicate partitioning of Te, Se, and S: Implications for earth differentiation. *Geochim. Cosmochim. Acta* **73**, 4598–4615 (2009).
8. Boujibar, A. *et al.* Metal-silicate partitioning of sulphur, new experimental and thermodynamic constraints on planetary accretion. *Earth Planet. Sci. Lett.* **391**, 42–54 (2014).
9. Suer, T.-A., Siebert, J., Remusat, L., Menguy, N. & Fiquet, G. A sulfur-poor terrestrial core inferred from metal–silicate partitioning experiments. *Earth Planet. Sci. Lett.* **469**, 84–97 (2017).
10. O'Neill, H. S. . The origin of the moon and the early history of the earth—A chemical model. Part 1: The moon. *Geochim. Cosmochim. Acta* **55**, 1135–1157 (1991).
11. Braukmüller, N., Wombacher, F., Funk, C. & Münker, C. Earth's volatile element depletion pattern inherited from a carbonaceous chondrite-like source. *Nat. Geosci.* **12**, 564–568 (2019).
12. Lodders, K. Solar System Abundances and Condensation Temperatures of the Elements. *Astrophys. J.* **591**, 1220–1247 (2003).
13. Wang, Z. & Becker, H. Ratios of S, Se and Te in the silicate Earth require a volatile-rich late veneer. *Nature* **499**, 328–331 (2013).
14. Yierpan, A., König, S., Labidi, J. & Schoenberg, R. Selenium isotope and S-Se-Te elemental systematics along the Pacific-Antarctic ridge: Role of mantle processes. *Geochim. Cosmochim. Acta* **249**, 199–224 (2019).
15. Labidi, J., Cartigny, P. & Moreira, M. Non-chondritic sulphur isotope composition of the terrestrial mantle. *Nature* **501**, 208–211 (2013).
16. Labidi, J., Cartigny, P., Hamelin, C., Moreira, M. & Dosso, L. Sulfur isotope budget (32S,33S,34S and36S) in Pacific-Antarctic ridge basalts: A record of

mantle source heterogeneity and hydrothermal sulfide assimilation. *Geochim. Cosmochim. Acta* **133**, 47–67 (2014).

17. Gao, X. & Thiemens, M. H. Isotopic composition and concentration of sulfur in carbonaceous chondrites. *Geochim. Cosmochim. Acta* **57**, 3159–3169 (1993).
18. Gao, X. & Thiemens, M. H. Variations of the isotopic composition of sulfur in enstatite and ordinary chondrites. *Geochim. Cosmochim. Acta* **57**, 3171–3176 (1993).
19. Labidi, J., Farquhar, J., Alexander, C. M. O. D., Eldridge, D. L. & Oduro, H. Mass independent sulfur isotope signatures in CMs: Implications for sulfur chemistry in the early solar system. *Geochim. Cosmochim. Acta* **196**, 326–350 (2017).
20. Labidi, J. *et al.* Experimentally determined sulfur isotope fractionation between metal and silicate and implications for planetary differentiation. *Geochim. Cosmochim. Acta* **175**, 181–194 (2016).
21. Fischer, R. A. *et al.* High pressure metal–silicate partitioning of Ni, Co, V, Cr, Si, and O. *Geochim. Cosmochim. Acta* **167**, 177–194 (2015).
22. Sanloup, C. *et al.* Structural change in molten basalt at deep mantle conditions. *Nature* **503**, 104–107 (2013).
23. Sun, N., Stixrude, L., Koker, N. de & Karki, B. B. First principles molecular dynamics simulations of diopside (CaMgSi2O6) liquid to high pressure. *Geochim. Cosmochim. Acta* **75**, 3792–3802 (2011).
24. De Koker, N. Structure, thermodynamics, and diffusion in CaAl2Si2O8 liquid from first-principles molecular dynamics. *Geochim. Cosmochim. Acta* **74**, 5657–5671 (2010).
25. McEwing, C. ., Thode, H. . & Rees, C. . Sulphur isotope effects in the dissociation and evaporation of troilite: A possible mechanism for 34S enrichment in lunar soils. *Geochim. Cosmochim. Acta* **44**, 565–571 (1980).
26. Young, E. D. *et al.* Near-equilibrium isotope fractionation during planetesimal evaporation. *Icarus* **323**, 1–15 (2019).
27. Bigeleisen, J. & Mayer, M. G. Calculation of Equilibrium Constants for Isotopic Exchange Reactions. *J. Chem. Phys.* **15**, 261 (1947).
28. Nash, W. M., Smythe, D. J. & Wood, B. J. Compositional and temperature effects on sulfur speciation and solubility in silicate melts. *Earth Planet. Sci. Lett.* **507**, 187–198 (2019).
29. Jugo, P. J., Wilke, M. & Botcharnikov, R. E. Sulfur K-edge XANES analysis of natural and synthetic basaltic glasses: Implications for S speciation and S content as function of oxygen fugacity. *Geochim. Cosmochim. Acta* **74**, 5926–5938 (2010).
30. Wadhwa, M. Redox Conditions on Small Bodies, the Moon and Mars. *Rev. Mineral. Geochemistry* **68**, 493–510 (2008).
31. McCammon, C. GEOCHEMISTRY: The Paradox of Mantle Redox. *Science*

(80-.). **308**, 807–808 (2005).

32. Rubie, D. C., Nimmo, F. & Melosh, H. J. Formation of the Earth's Core. in *Treatise on Geophysics* 43–79 (Elsevier, 2015). doi:10.1016/B978-0-444-53802-4.00154-8.
33. Righter, K. Prediction of metal-silicate partition coefficients for siderophile elements: An update and assessment of PT conditions for metal-silicate equilibrium during accretion of the Earth. *Earth Planet. Sci. Lett.* **304**, 158–167 (2011).
34. Rubie, D. C. *et al.* Accretion and differentiation of the terrestrial planets with implications for the compositions of early-formed Solar System bodies and accretion of water. *Icarus* **248**, 89–108 (2015).
35. Grewal, D. S., Dasgupta, R., Sun, C., Tsuno, K. & Costin, G. Delivery of carbon, nitrogen, and sulfur to the silicate Earth by a giant impact. *Sci. Adv.* **5**, eaau3669 (2019).
36. Varas-Reus, M. I., König, S., Yierpan, A., Lorand, J.-P. & Schoenberg, R. Selenium isotopes as tracers of a late volatile contribution to Earth from the outer Solar System. *Nat. Geosci.* **12**, 779–782 (2019).
37. Sharp, Z. D. Nebular ingassing as a source of volatiles to the Terrestrial planets. *Chem. Geol.* **448**, 137–150 (2017).
38. McDonough, W. F. & Sun, S. -s. The composition of the Earth. *Chem. Geol.* **120**, 223–253 (1995).
39. Mann, U., Frost, D. J., Rubie, D. C., Becker, H. & Audétat, A. Partitioning of Ru, Rh, Pd, Re, Ir and Pt between liquid metal and silicate at high pressures and high temperatures - Implications for the origin of highly siderophile element concentrations in the Earth's mantle. *Geochim. Cosmochim. Acta* **84**, 593–613 (2012).
40. Nie, N. X. & Dauphas, N. Vapor Drainage in the Protolunar Disk as the Cause for the Depletion in Volatile Elements of the Moon. *Astrophys. J.* **884**, L48 (2019).
41. Wang, K. & Jacobsen, S. B. Potassium isotopic evidence for a high-energy giant impact origin of the Moon. *Nature* **538**, 487–490 (2016).
42. Paniello, R. C., Day, J. M. D. & Moynier, F. Zinc isotopic evidence for the origin of the Moon. *Nature* **490**, 376–379 (2012).
43. Lock, S. J. *et al.* The Origin of the Moon Within a Terrestrial Synestia. *J. Geophys. Res. Planets* **123**, 910–951 (2018).
44. Schaefer, L., Lodders, K. & Fegley, B. VAPORIZATION OF THE EARTH: APPLICATION TO EXOPLANET ATMOSPHERES. *Astrophys. J.* **755**, 41 (2012).
45. Day, J. M. D. Geochemical constraints on residual metal and sulfide in the sources of lunar mare basalts. *Am. Mineral.* **103**, 1734–1740 (2018).
46. Saal, A. E. & Hauri, E. H. Large sulfur isotope fractionation in lunar volcanic glasses reveals the magmatic differentiation and degassing of the Moon. *Sci.*

Adv. **7**, 1–12 (2021).

47. Wing, B. A. & Farquhar, J. Sulfur isotope homogeneity of lunar mare basalts. *Geochim. Cosmochim. Acta* **170**, 266–280 (2015).

48. Franz, H. B. *et al.* Isotopic links between atmospheric chemistry and the deep sulphur cycle on Mars. *Nature* **508**, 364–368 (2014).

49. Rai, V. K., Jackson, T. L. & Thiemens, M. H. Photochemical mass-independent sulfur isotopes in achondritic meteorites. *Science* **309**, 1062–5 (2005).

50. Wu, N., Farquhar, J., Dottin, J. W. & Magalhães, N. Sulfur isotope signatures of eucrites and diogenites. *Geochim. Cosmochim. Acta* **233**, 1–13 (2018).

51. Defouilloy, C., Cartigny, P., Assayag, N., Moynier, F. & Barrat, J.-A. High-precision sulfur isotope composition of enstatite meteorites and implications of the formation and evolution of their parent bodies. *Geochim. Cosmochim. Acta* **172**, 393–409 (2016).

52. Antonelli, M. A. *et al.* Early inner solar system origin for anomalous sulfur isotopes in differentiated protoplanets. *Proc. Natl. Acad. Sci.* **111**, 17749–17754 (2014).

53. Dottin, J. W., Farquhar, J. & Labidi, J. Multiple sulfur isotopic composition of main group pallasites support genetic links to IIIAB iron meteorites. *Geochim. Cosmochim. Acta* **224**, 276–281 (2018).

Methods

Equilibrium isotope fractionation factor

Bigeleisen–Mayer equation[27] has been widely used to calculate the reduced partition function ratio (β) of element X in phase A, which represents the equilibrium isotope fractionation factor of element X between the phase A and an ideal gas of X atoms. Under the high-temperature approximation, the Bigeleisen–Mayer equation can be expressed as:

$$\beta = 1 + \left(\frac{1}{m} - \frac{1}{m'}\right)\frac{\hbar^2}{24k^2T^2}(f_{xx} + f_{yy} + f_{zz}) \tag{1}$$

where m and m' refer to the light and heavy isotopes, respectively; f_{xx}, f_{yy}, and f_{zz} are the diagonal elements of the force constant matrix; T is temperature in Kelvin, and $\hbar$ and k are the reduced Planck constant and Boltzmann constant, respectively. Thus, the equilibrium isotope fractionation factor between phase A and B can be derived from:

$$10^3 ln\alpha_{A-B} = 10^3 ln\beta_A - 10^3 ln\beta_B = \left(\frac{1}{m} - \frac{1}{m'}\right)\frac{\hbar^2}{8k^2T^2}(<F>_A - <F>_B) \tag{2}$$

Here $<F>$ is defined as the average value of diagonal elements of the force constant matrix $(f_{xx} + f_{yy} + f_{zz})/3$. The use of Eq. (2) requires the validity criteria that frequencies related to the element of interest ω_i (cm^{-1}) ≤ 1.39 T (T is the temperature in Kelvin). For the temperature of core formation (> 3000 K), the upper limit of frequencies is > 4200 cm^{-1}, which is higher than any vibrational frequency associated with S atom in secular materials. This method has been also successfully applied to predict the equilibrium barium isotope fractionation between minerals and aqueous solution at low temperature[54] and the nickel isotope fractionation between silicate and metallic melts[55].

First-principles molecular dynamics simulations

Equilibrium sulfur (S) isotope fractionation factors between silicate and metallic melts can be estimated from the <F> difference between these two melts using Eq. (2). Because melts do not have regular structures as solid crystals, we conducted first-principles molecular dynamics (FPMD) simulations based on the density functional theory (DFT) using VASP with the projector-augmented wave (PAW) method[56] to predict the structures of S-bearing silicate and metallic melts. The generalized-gradient approximation (GGA)[57] was adopted for the exchange-correlation functional and the PBE pseudopotentials were used. The energy cutoff for the plane wave was 600 eV. The Brillouin zone summations over the electronic states were performed at gamma point. Here we firstly focus on three different melts, including metallic melt with a chemical formula of $Fe_{97}S_3$ and two silicate melts with chemical formulas of $Mg_{32}Si_{32}O_{95}S$ and $Mg_{32}Si_{32}O_{96}SO_2$. The former silicate melt represents the S-bearing silicate melt under relatively reducing condition and the latter refers to relatively oxidizing condition. The chemical composition of $MgSiO_3$ was chosen for silicate melts because it has similar MgO and SiO_2 contents to primitive chondrites. In order to check the effect of other minor elements on the structural properties obtained for S in silicate and metallic melt, we also conducted FPMD simulations on a pyrolitic composition ($Mg_{41}Ca_2Fe_5Si_{32}Al_4O_{117}S$) and a multicomponent alloy ($Fe_{87}Ni_4Si_{10}O_2C_2S_3$) under relatively reducing condition. All FPMD simulations were performed in the NVT thermodynamic ensemble with a fixed temperature controlled by a Nosé thermostat. The simulations for Fe-bearing systems are spin - polarized, with the spin on each Fe atom being allowed to freely fluctuate at each step. We did not introduce a Hubbard U correction for Fe atoms in our calculations. Caracas et al.[58] checked the behavior of the Fe-bearing melt based on DFT+U and found that a +U correction does not significantly change the calculated results. Cell parameters and volumes of simulated boxes are listed in Supplementary Table 1. The time step was set to be 1 fs and the initial liquid configurations at different volumes were prepared by melting the structures at 6000 K for 20 ps. After that, all simulations were conducted at 3000 K for at least 60 ps. Pressures at different volumes can be derived by averaging the pressure for each time step after the equilibration.

To obtain the force constant of S atom in silicate and metallic melts, large numbers of snapshots were extracted from the FPMD trajectories every 250 steps after equilibration for the single-atom optimization, in which only S atomic positions were relaxed with fixed cubic boxes. Then the force constant matrix of S in each snapshot can be calculated using the small displacement method (see Supplementary Information) and the statistical average on all snapshots is the average force constant of S atom in the melts.

Our results suggest the Si-O distance initially increases from ~ 1.62 Å at 6.28 GPa to ~ 1.67 Å at 66.85 GPa and then maintains at ~ 1.66 Å with further compression (Supplementary Fig. 1 and 2), whereas the Mg-O bond length significantly decreases from 1.97 to 1.88 Å when the pressure increases from 6.28 GPa to 105.03 GPa. Meanwhile, the coordination numbers (CNs) for Si-O and Mg-O pairs increase from ~ 4.1 to 6 and from ~ 4.1 to 7.1 at that pressure range (Supplementary Fig. 1 and 2), respectively. The calculated structural properties agree well with previous experimental measurements[22] and theoretical studies[23,24], ensuring the accuracy and reliability of our calculations. In $Mg_{32}Si_{32}O_{96}SO_2$ melt, the S-O distance (~ 1.5 Å) is much shorter than the S-Mg (> 2.5 Å) and S-Si distances (> 2.8 Å) and the coordination number (CN) for S-O pair is ~3 if the cutoff is 2.0 Å (Extended Data Fig. 1), suggesting that S atom is directly bonded to O atoms as sulfate under relatively oxidizing conditions. In contrast, the S-O distance in $Mg_{32}Si_{32}O_{95}S$ melt (~2.6 Å) is much longer than that in the $Mg_{32}Si_{32}O_{96}SO_2$ melt, while the S-Mg (~2.4 Å) and S-Si distances (~2.05 Å) are much shorter than those in $Mg_{32}Si_{32}O_{96}SO_2$ melt (Extended Data Fig. 2). When the cutoff for the coordination shell is 2.5 Å, the CNs for S-Mg and S-Si pairs are both ~1, suggesting that the S atom is bonded to Si and Mg atoms, which is self-consistent with the valence state of S (S^{2-}). The S atom in $Mg_{41}Ca_2Fe_5Si_{32}Al_4O_{117}S$ melt is preferentially bonded to Fe and Mg atoms (Extended Data Fig. 4), but the S-Fe distance (~ 2.10 Å) is shorter than the S-Mg distance (~ 2.37 Å). The CNs for S-Fe and S-Mg pairs are ~2 and 1, respectively, when the cutoff for the coordination shell is 2.5 Å. In $Fe_{97}S_3$ melt, the S-Fe distance (2.09-2.15 Å) is comparable to the S-Fe distance in

$Mg_{41}Ca_2Fe_5Si_{32}Al_4O_{117}S$ melt and the CNs are 4-5 if the cutoff is 2.4 Å (Extended Data Fig. 3). In $Fe_{87}Ni_4Si_{10}O_2C_2S_3$ melt, the S atom is dominantly bonded to Fe and Ni atoms with a S-Fe/Ni distance of ~2.11 Å (Extended Data Fig. 4), similar to the S-Fe distance in $Fe_{97}S_3$ melt.

The <F> of S in each snapshot and the statistical average are shown in Supplementary Fig. 3-6. Our results show that the <F> difference between silicate and metallic melts is smaller than 25 N/m at < 80 GPa (Extended Data Fig. 5 and Supplementary Table 1) when S^{2-} is the dominant species, suggesting no significant equilibrium S isotope fractionation between these two phases (Fig. 2). The <F> of S in $Mg_{41}Ca_2Fe_5Si_{32}Al_4O_{117}S$ and $Fe_{87}Ni_4Si_{10}O_2C_2S_3$ melts are 291.6 N/m at 46.6 GPa and 253.8 N/m at 41.8 N/m, which are only ~15 N/m higher than the values for $Mg_{32}Si_{32}O_{95}S$ and $Fe_{97}S_3$ systems (Extended Data Fig. 5). This indicates that the presence of other components does not significantly affect the the $10^3\ln\alpha$ between silicate and metallic melts under relatively reducing condition. Previous experimental work argued that Fe metal is preferentially enriched in ^{34}S relative to silicate melt and the fractionation is up to +0.64 ‰ at 1923 K. If this is correct, the <*F*> of S in silicate melt should be at least 290 N/m lower than that the one in metallic melt, which deviates from the direction of our predictions. This is likely because the isotope exchange during experiments had not reached the equilibrium state.

Sulfur species in vapor phases

In order to estimate the equilibrium S isotope fractionation between the vapor phase and silicate melt, we first determined the S species in the vapor phase. We used the GRAINS code[59] to calculate the minimum Gibbs free energy of the system with solar abundance for the elements[12] at specific temperature and $1e^{-4}$ bar. This code considered 33 elements (H, He, C, N, O, Na, Mg, Al, Si, P, S, Cl, K, Ca, Ti, Cr, Mn, Fe, Co, Ni, Cu, Ga, Ge, Mo, Ru, Pd, Hf, W, Re, Os, Ir, Pt, Au). The code considers 242 gas species and 520 condensed (liquid or solid) species freely and outputs all the species when the system achieves chemical equilibrium through Gibbs free energy minimization. We used the solar abundances for the elements to calculate the equilibrium gas phases because the solar nebular would not have completely dissipated during planetesimal evaporation in the first several million years[37]. The evaporation of planetesimals investigated here requires the presence of nebular H_2 under a total pressure of $1e^{-4}$ bar. The results of all S species at 1000-1600 K and $1e^{-4}$ bar are listed in Supplementary Table 2. The important species for S in the vapor includes H_2S (g), HS (g), SiS (g), and S_2 (g), among which the fraction of H_2S is the largest at 1000-1500 K. To check the effect of H concentration on the S species in the vapor phase, we also conducted thermodynamic calculations using GRAINS with solar elemental abundances but with H concentration decreased by one and four orders of magnitude, conditions that are more oxidizing than the solar nebular. The results show that S in the vapor phase mainly occurs as H_2S and/or HS at 1000-1500 K when H concentration is decreased by 90%, while SO, SO_2, and S_2 are the main S species when only 0.01% H is retained (Extended Data Fig. 7). On the basis of these results, we conducted first-principles calculations for these S species in the vapor phase. For each S species, we put a molecule in a cubic box (20 Å×20 Å×20 Å) and relaxed the atomic positions. The <F> of S can be estimated using the small displacement method (Supplementary Table 1). We checked the effect of box size and found that the results will not change with the size when the cell parameter is larger than 20 Å. The atomic S gas has a <F> of 0 N/m and the β factor is 0, because there is no atomic bonding in this system. Thus, the <F> of S in the vapor with the presence of nebular H_2 can be calculated based on the fractions of each species (Supplementary Table 2).

Isotope fractionation during evaporation and condensation

Young et al.[26] investigated the nature of evaporation process and how evaporation and condensation fractionate isotopes using numerical simulations. Following that work, the S isotope fractionation during evaporation and condensation ($\Delta^{34}S_{\text{vapor-melt}}$)

can be approximately expressed as:

$$\Delta^{34}S_{\text{vapor-melt}}=\Delta^{34}S^{eq}+(1-D)*\Delta^{34}S^{kin} \quad (3)$$

where $\Delta^{34}S^{eq}$ is the equilibrium S isotope fractionation between vapor phase and melt, $\Delta^{34}S^{kin}$ is the kinetic S isotope fractionation, and D is the degree vapor saturation ($D=P/P_{sat}$, P is the pressure of the evaporating species at the surface of the melt and P_{sat} is the saturation vapor pressure). $\Delta^{34}S^{kin}$ can be estimated from: $\Delta^{34}S^{kin} = 1000*[(m_{S32}/m_{S34})^{1/2} - 1]$, where is the atomic or molecular mass of the vapor species. This simplified approach gives the instantaneous isotopic fractionation between vapor and melt.

The effect of planetesimal evaporation on the $\delta^{34}S$ of proto-Earth and other differentiated bodies depends on the degree vapor saturation and S species in the vapor phase that are a function of oxygen fugacity and temperature. If D is lower than 100%, the net evaporation fractionation factor of S isotopes ($\Delta^{34}S_{\text{vapor-melt}}$) would be affected by the large negative kinetic fractionation, and the final $\Delta^{34}S_{\text{vapor-melt}}$ could be positive, zero, or negative even when the S evaporates mainly as H_2S from planetesimals. On the other hand, when D is 100%, $\Delta^{34}S_{\text{vapor-melt}}$ is controlled by the S species in the vapor phase. The evaporation of atomic S will enrich the melt in heavy S isotopes, whereas H_2S evaporation will enrich the melt in light S isotopes.

Differentiated planetesimals may have undergone S evaporation under a range of conditions, which may show different effects on their $\delta^{34}S$ values. When planetesimals undergo evaporation in the presence of nebular H_2 under a total pressure of about 10^{-4} bar, numerical simulations[26] show that the vapor saturation degree will be approximately 100%, and the net isotope fractionation is equal to the equilibrium isotope fractionation between vapor and melt. The evaporation of planetesimal melts in the presence of nebular H_2 can also explain the Mg and Si isotopic and elemental compositions of the bulk Earth[26]. The observed bulk Earth S isotope signature and abundance can be reproduced by the evaporative loss of ~90% S, mainly as H_2S, from molten planetesimals in a H_2 atmosphere. For Mars, previous studies reported that most sulfides in shergotiites have negative $\delta^{34}S$ values, indicating that the Martian mantle is also likely to have a negative $\delta^{34}S$ value. The average S concentration for all shergotiites[48] is about four times the S abundance in the BSE. As such, the evaporative loss of S (~60%) would be significantly lower than the estimate for Earth and the effect of evaporation on the $\delta^{34}S$ value ($\Delta^{34}S_{\text{Mars-chondrites}}=\Delta^{34}S^{eq}_{\text{vapor-melt}}*\ln f$, where f is the S fraction remaining) would be smaller than that for Earth. So overall, the literature data of sulfides in shergotiites primary supports our conclusions.

References

54. Wang, W., Wu, Z. & Huang, F. Equilibrium barium isotope fractionation between minerals and aqueous solution from first-principles calculations. *Geochim. Cosmochim. Acta* **292**, 64–77 (2021).
55. Wang, S.-J. *et al.* Nickel isotopic evidence for late-stage accretion of Mercury-like differentiated planetary embryos. *Nat. Commun.* **12**, 294 (2021).
56. Blöchl, P. E. Projector augmented-wave method. *Phys. Rev. B* **50**, 17953–17979 (1994).
57. Perdew, J. P., Burke, K. & Ernzerhof, M. Generalized Gradient Approximation Made Simple. *Phys. Rev. Lett.* **77**, 3865–3868 (1996).
58. Caracas, R., Hirose, K., Nomura, R. & Ballmer, M. D. Melt–crystal density crossover in a deep magma ocean. *Earth Planet. Sci. Lett.* **516**, 202–211 (2019).
59. Petaev, M. I. The GRAINS thermodynamic and kinetic code for modeling nebular condensation. *Calphad* **33**, 317–327 (2009).

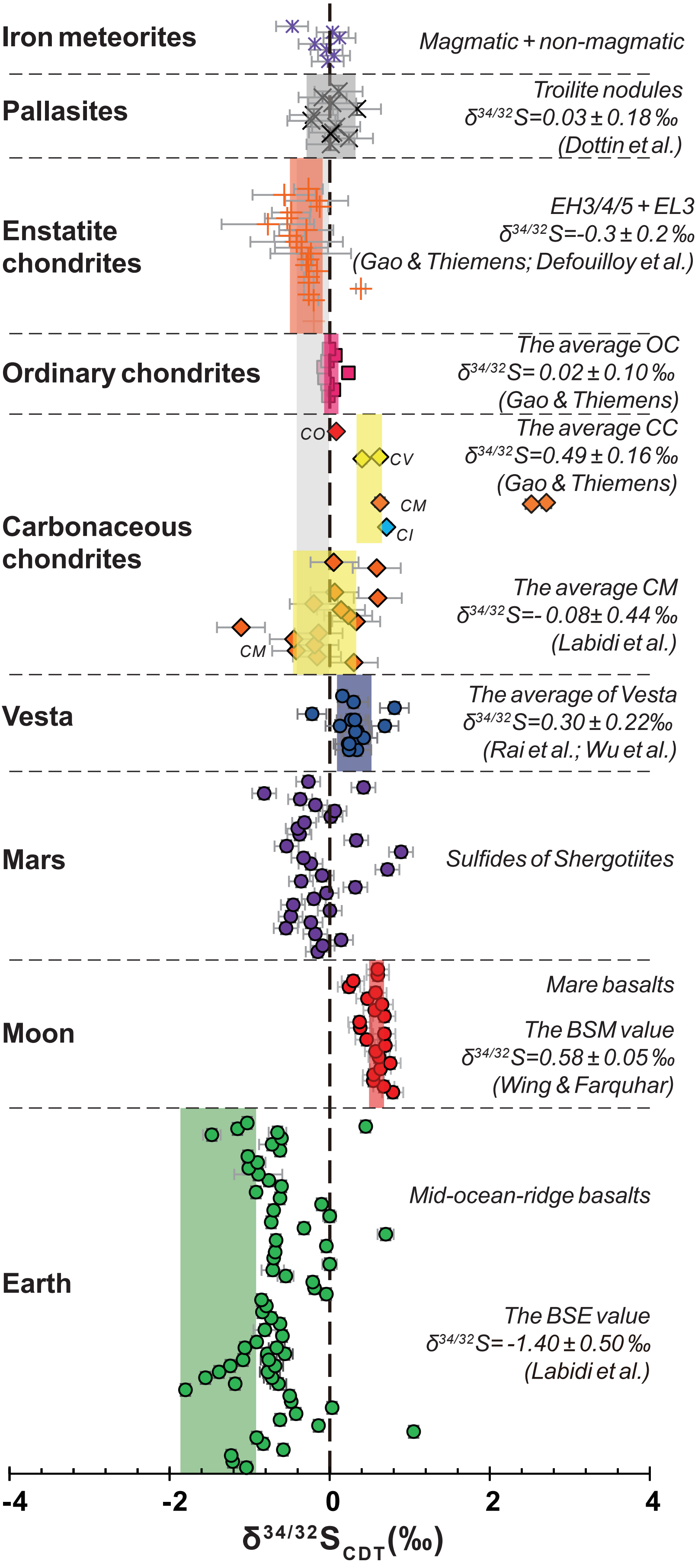
Iron meteorites
Magmatic + non-magmatic
Pallasites
Troilite nodules
δ34/32S=0.03 ± 0.18 ‰
(Dottin et al.)
Enstatite chondrites
EH3/4/5 + EL3
δ34/32S=-0.3 ± 0.2 ‰
(Gao & Thiemens; Defouilloy et al.)
Ordinary chondrites
The average OC
δ34/32S= 0.02 ± 0.10 ‰
(Gao & Thiemens)
CO
CV
The average CC
δ34/32S=0.49 ± 0.16 ‰
(Gao & Thiemens)
CM
CI
Carbonaceous chondrites
The average CM
δ34/32S=- 0.08± 0.44 ‰
(Labidi et al.)
CM
Vesta
The average of Vesta
δ34/32S=0.30 ± 0.22‰
(Rai et al.; Wu et al.)
Mars
Sulfides of Shergotiites
Moon
Mare basalts
The BSM value
δ34/32S=0.58 ± 0.05 ‰
(Wing & Farquhar)
Earth
Mid-ocean-ridge basalts
The BSE value
δ34/32S= -1.40 ± 0.50 ‰
(Labidi et al.)
-4
-2
0
2
4
δ34/32SCDT (‰)

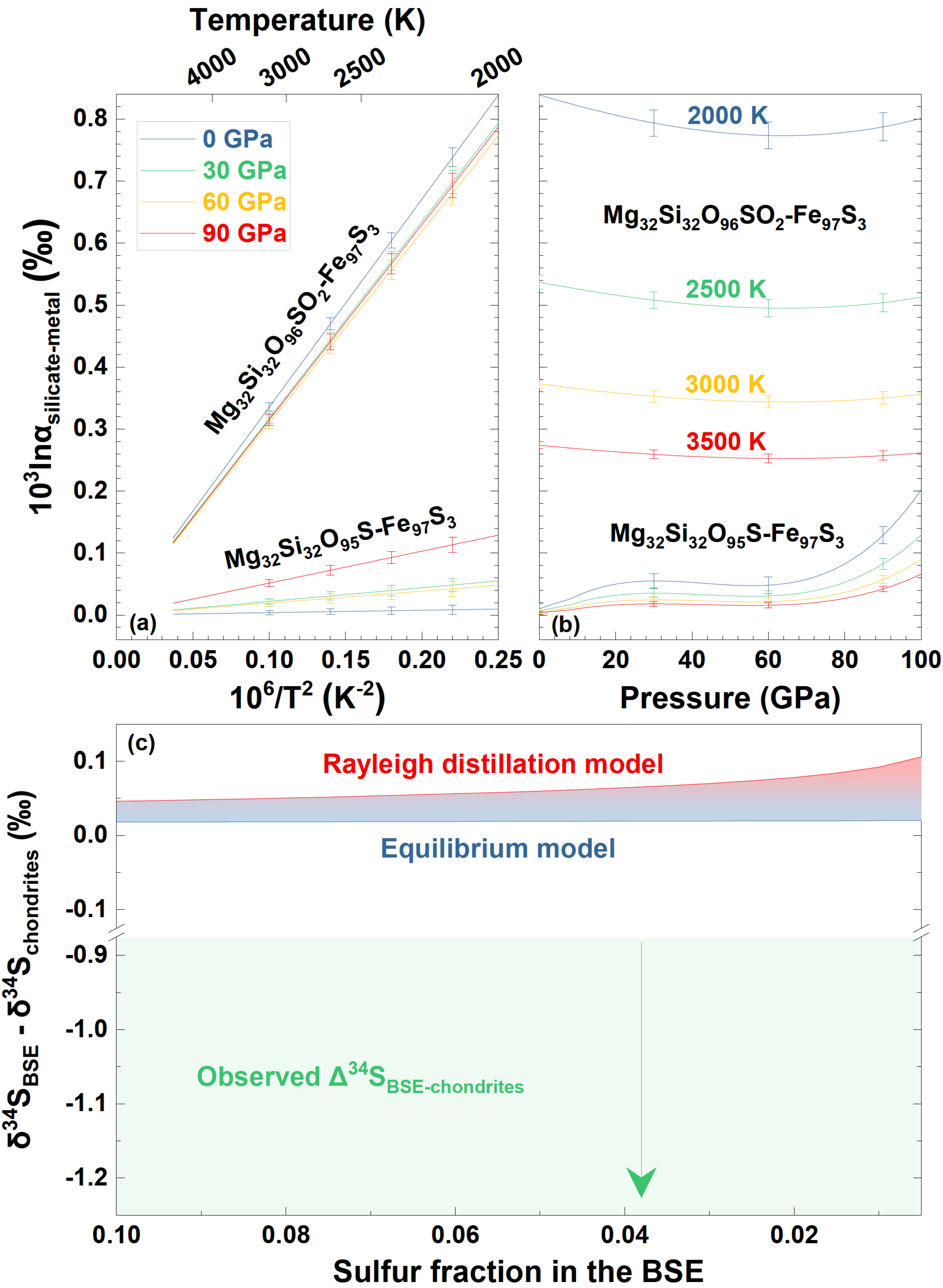
Temperature (K)
4000
3000
2500
2000
0 GPa
30 GPa
60 GPa
90 GPa
Mg32Si32O96SO2-Fe97S3
Mg32Si32O95S-Fe97S3
10^3 lnα_silicate-metal (‰)
0.8
0.7
0.6
0.5
0.4
0.3
0.2
0.1
0.0
(a)
0.00
0.05
0.10
0.15
0.20
0.25
10^6/T^2 (K^-2)
2000 K
2500 K
3000 K
3500 K
Mg32Si32O96SO2-Fe97S3
Mg32Si32O95S-Fe97S3
(b)
0
20
40
60
80
100
Pressure (GPa)
(c)
Rayleigh distillation model
Equilibrium model
Observed Δ34S_BSE-chondrites
δ34S_BSE - δ34S_chondrites (‰)
0.1
0.0
-0.1
-0.9
-1.0
-1.1
-1.2
0.10
0.08
0.06
0.04
0.02
Sulfur fraction in the BSE

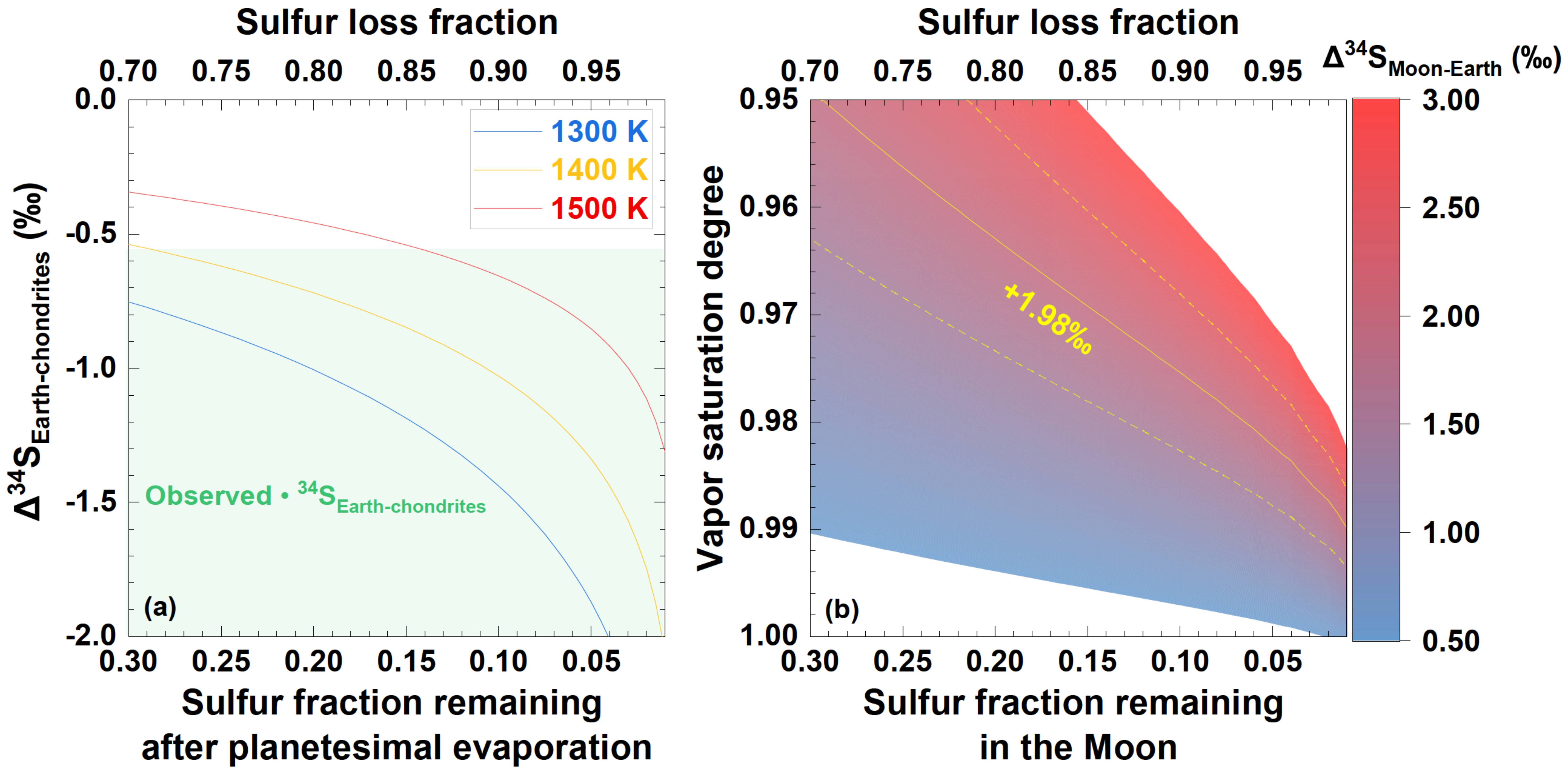
Sulfur loss fraction
0.70
0.75
0.80
0.85
0.90
0.95
0.0
-0.5
-1.0
-1.5
-2.0
$\Delta^{34}S_{Earth-chondrites}$ (‰)
1300 K
1400 K
1500 K
Observed • $^{34}S_{Earth-chondrites}$
(a)
0.30
0.25
0.20
0.15
0.10
0.05
Sulfur fraction remaining after planetesimal evaporation
Sulfur loss fraction
0.70
0.75
0.80
0.85
0.90
0.95
$\Delta^{34}S_{Moon-Earth}$ (‰)
0.95
0.96
0.97
0.98
0.99
1.00
Vapor saturation degree
+1.98‰
(b)
3.00
2.50
2.00
1.50
1.00
0.50
0.30
0.25
0.20
0.15
0.10
0.05
Sulfur fraction remaining in the Moon

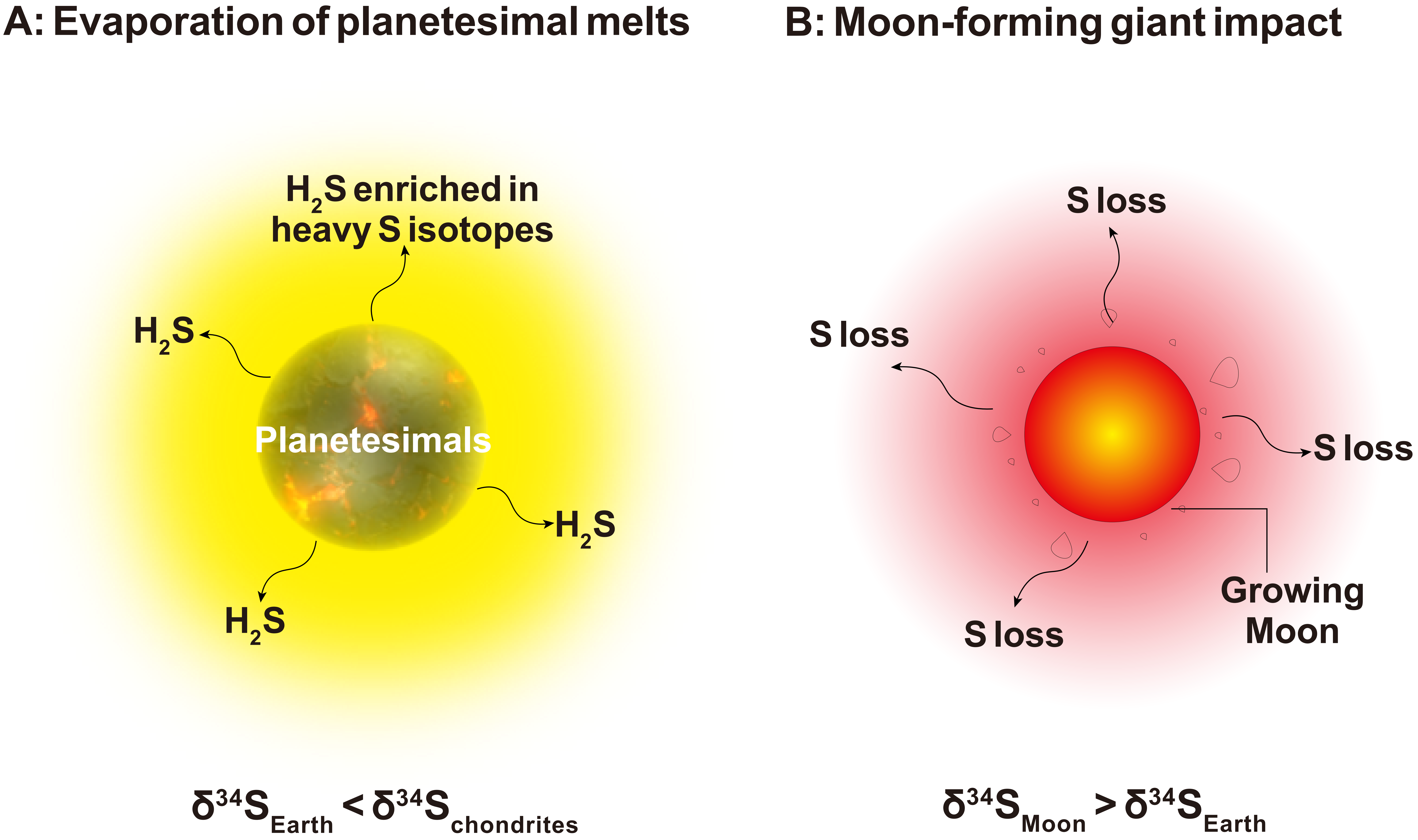
A: Evaporation of planetesimal melts
B: Moon-forming giant impact
H_2S enriched in heavy S isotopes
H_2S
Planetesimals
H_2S
H_2S
S loss
S loss
S loss
S loss
Growing Moon
$\delta^{34}S_{Earth} < \delta^{34}S_{chondrites}$
$\delta^{34}S_{Moon} > \delta^{34}S_{Earth}$

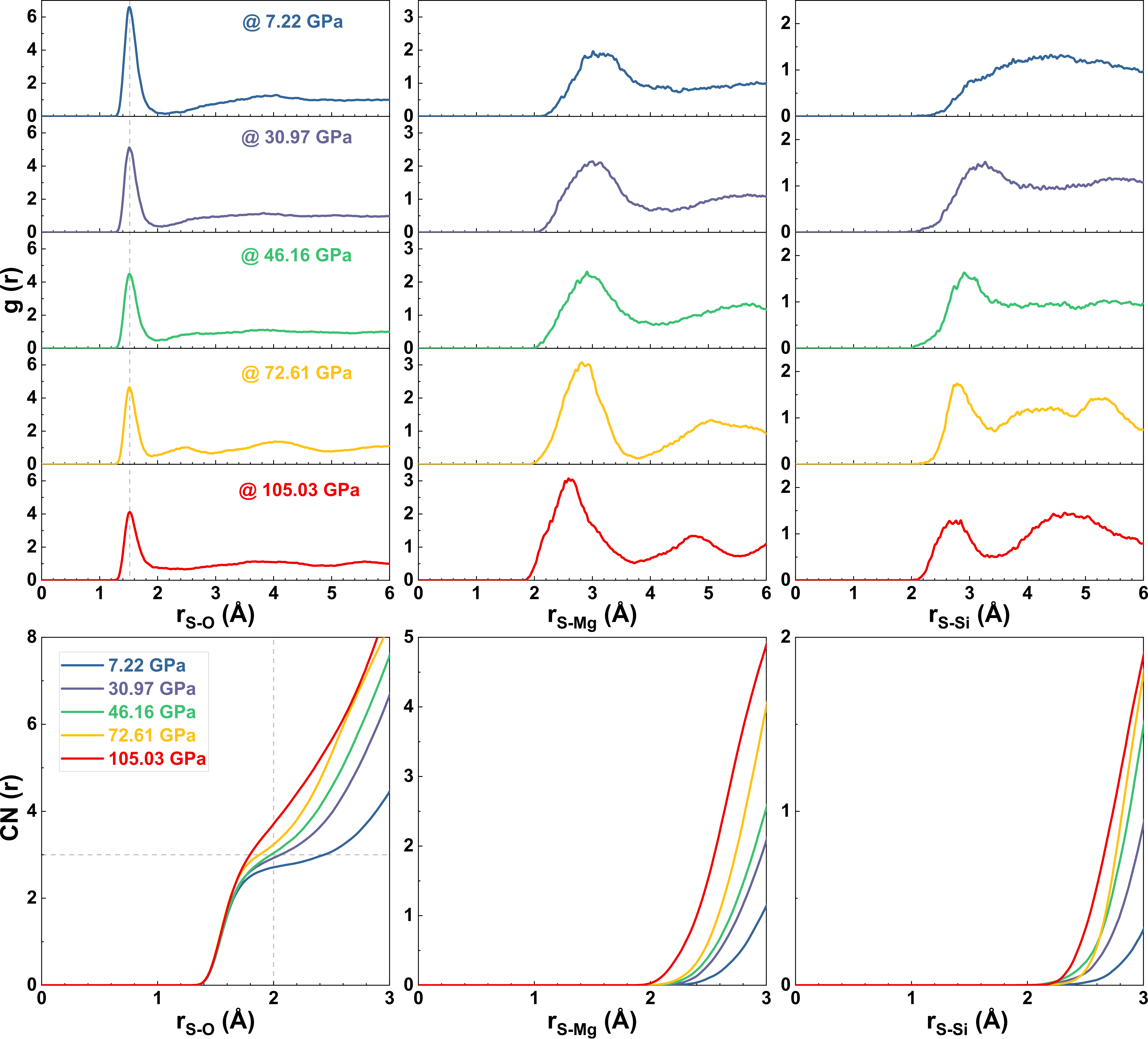
@ 7.22 GPa
@ 30.97 GPa
@ 46.16 GPa
@ 72.61 GPa
@ 105.03 GPa
g (r)
0
2
4
6
1
3
r_S-O (Å)
r_S-Mg (Å)
r_S-Si (Å)
0
1
2
3
4
5
6
CN (r)
8
7.22 GPa
30.97 GPa
46.16 GPa
72.61 GPa
105.03 GPa

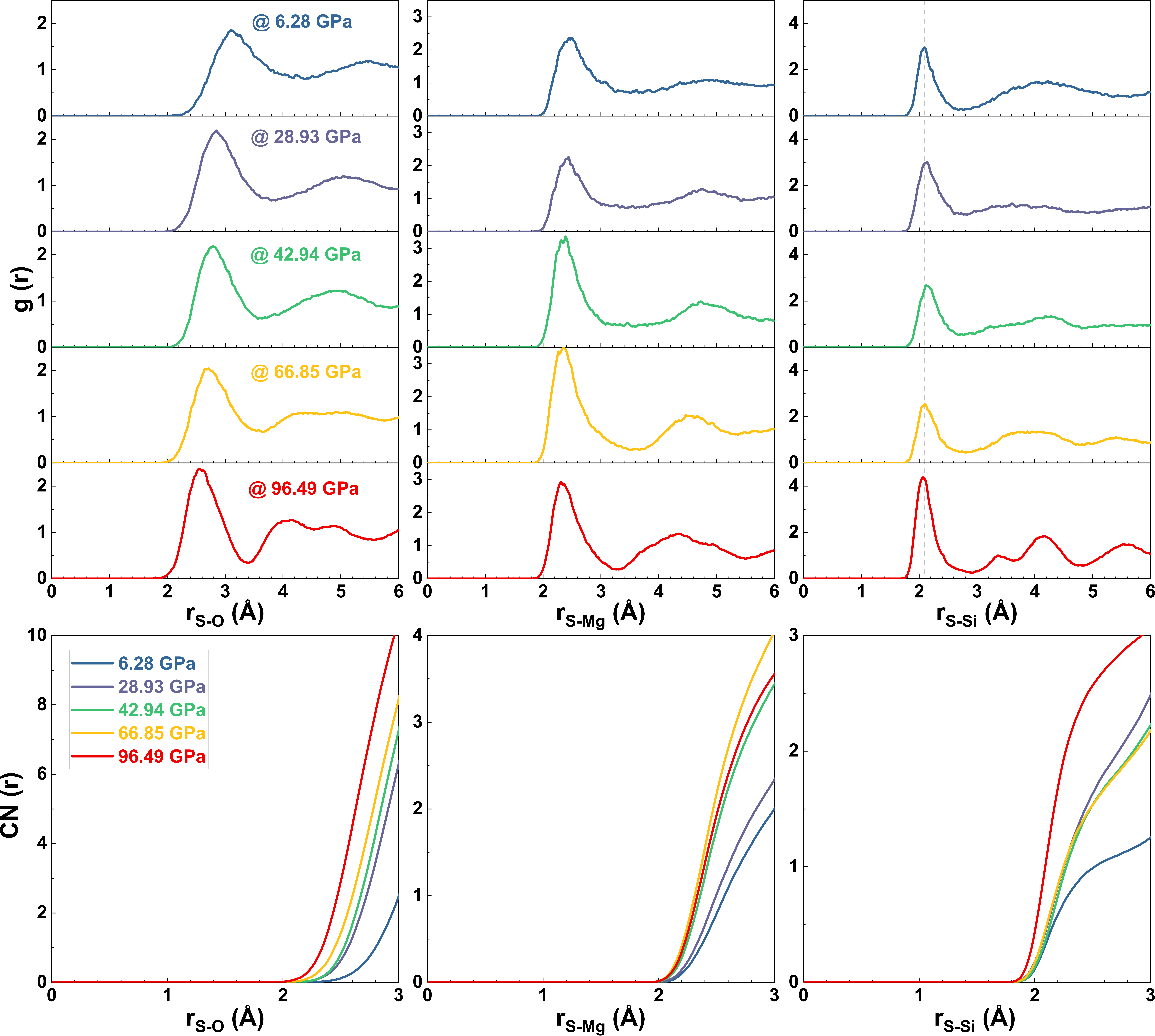
@ 6.28 GPa
@ 28.93 GPa
@ 42.94 GPa
@ 66.85 GPa
@ 96.49 GPa
g (r)
$r_{S\text{-}O}$ (Å)
$r_{S\text{-}Mg}$ (Å)
$r_{S\text{-}Si}$ (Å)
CN (r)
6.28 GPa
28.93 GPa
42.94 GPa
66.85 GPa
96.49 GPa
$r_{S\text{-}O}$ (Å)
$r_{S\text{-}Mg}$ (Å)
$r_{S\text{-}Si}$ (Å)

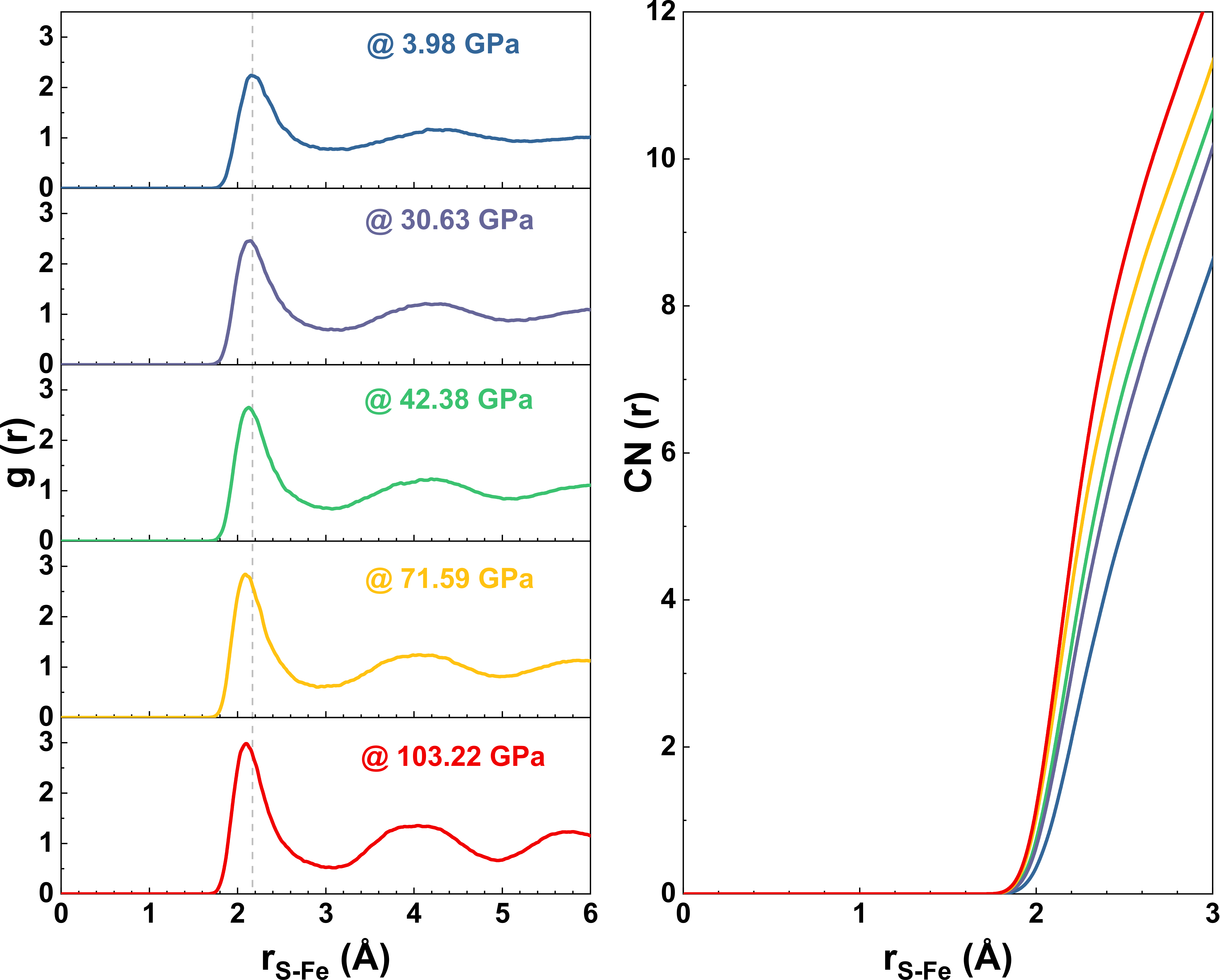
@ 3.98 GPa
@ 30.63 GPa
@ 42.38 GPa
@ 71.59 GPa
@ 103.22 GPa
g (r)
0
1
2
3
0
1
2
3
4
5
6
$r_{S\text{-}Fe}$ (Å)
CN (r)
0
2
4
6
8
10
12
0
1
2
3
$r_{S\text{-}Fe}$ (Å)

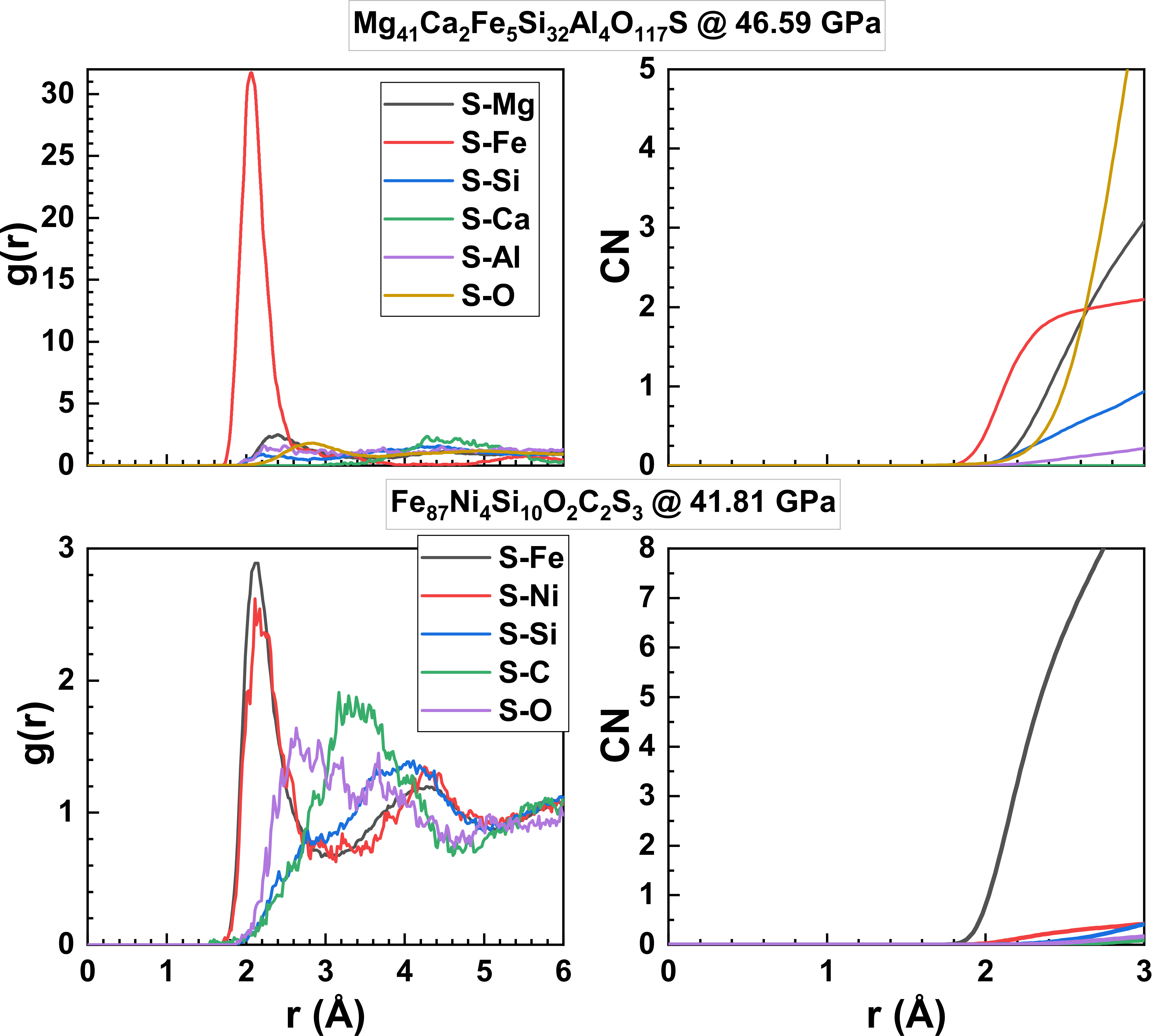
$Mg_{41}Ca_2Fe_5Si_{32}Al_4O_{117}S$ @ 46.59 GPa
g(r)
0
5
10
15
20
25
30
S-Mg
S-Fe
S-Si
S-Ca
S-Al
S-O
CN
0
1
2
3
4
5
$Fe_{87}Ni_4Si_{10}O_2C_2S_3$ @ 41.81 GPa
g(r)
0
1
2
3
S-Fe
S-Ni
S-Si
S-C
S-O
CN
0
1
2
3
4
5
6
7
8
0
1
2
3
4
5
6
r (Å)
0
1
2
3
r (Å)

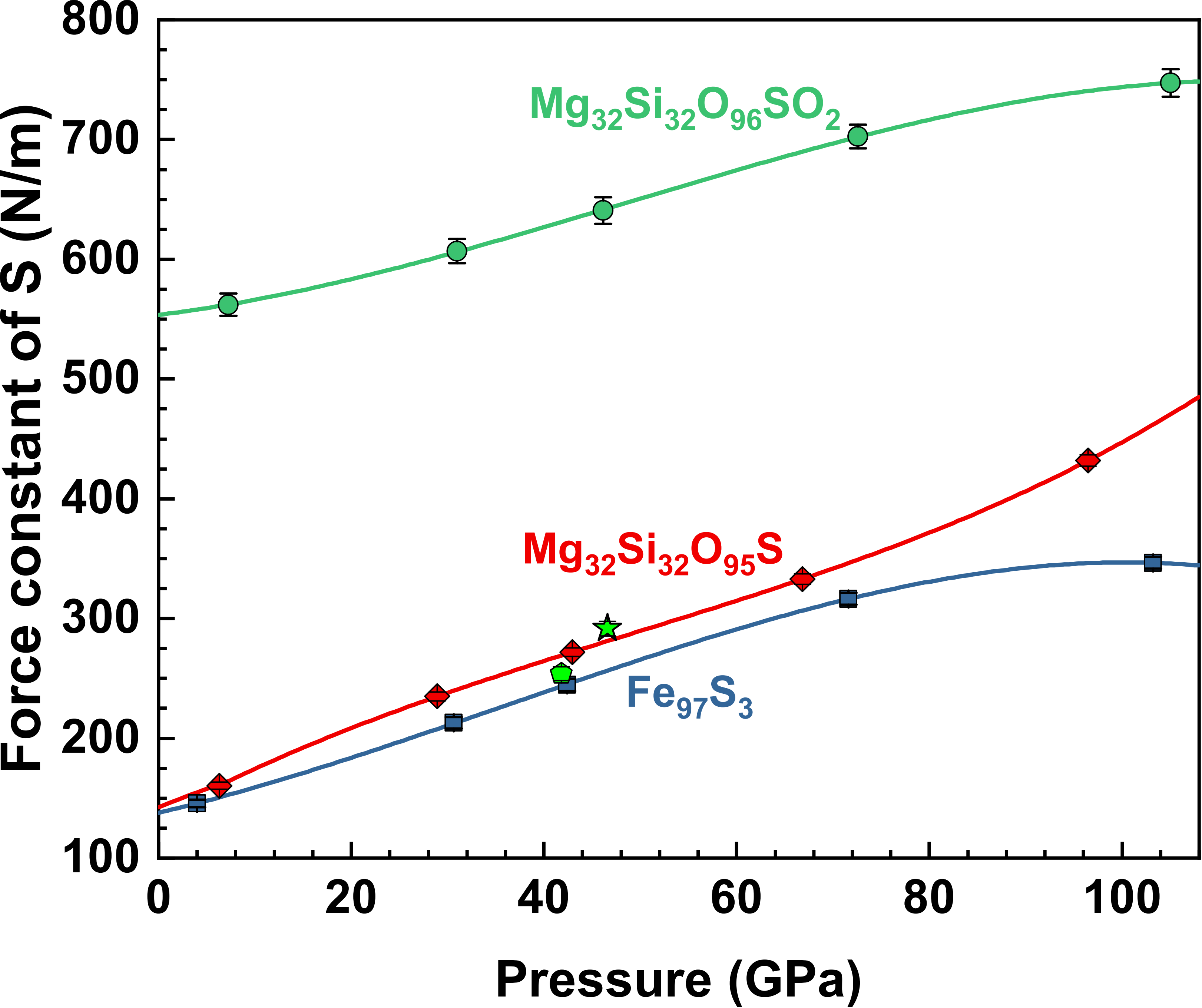
Force constant of S (N/m)
800
700
600
500
400
300
200
100
0
20
40
60
80
100
Pressure (GPa)
$Mg_{32}Si_{32}O_{96}SO_2$
$Mg_{32}Si_{32}O_{95}S$
$Fe_{97}S_3$

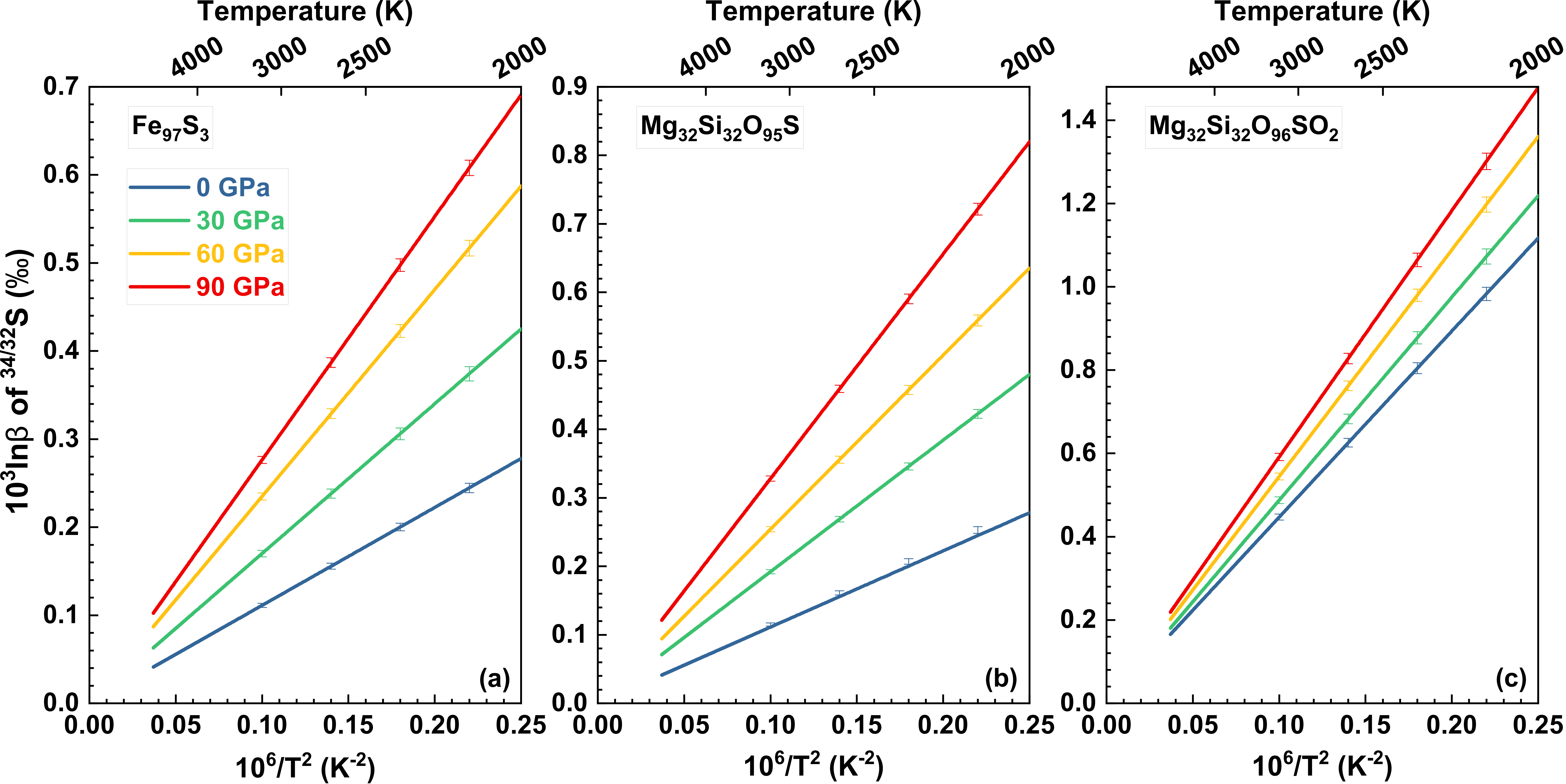
Temperature (K)
4000
3000
2500
2000
$10^3\ln\beta$ of $^{34/32}$S (‰)
$10^6/T^2$ (K^{-2})
$Fe_{97}S_3$
0 GPa
30 GPa
60 GPa
90 GPa
(a)
$Mg_{32}Si_{32}O_{95}S$
(b)
$Mg_{32}Si_{32}O_{96}SO_2$
(c)
0.0
0.1
0.2
0.3
0.4
0.5
0.6
0.7
0.8
0.9
1.0
1.2
1.4
0.00
0.05
0.10
0.15
0.20
0.25

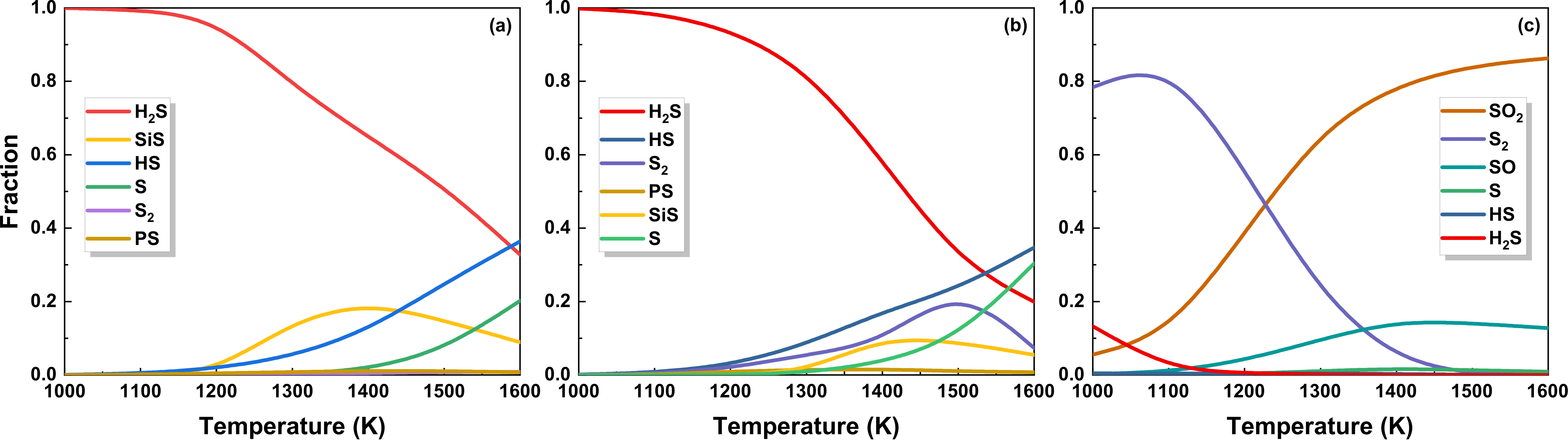
(a)
(b)
(c)
Fraction
Temperature (K)
1.0
0.8
0.6
0.4
0.2
0.0
1000
1100
1200
1300
1400
1500
1600
H_2S
SiS
HS
S
S_2
PS
H_2S
HS
S_2
PS
SiS
S
SO_2
S_2
SO
S
HS
H_2S

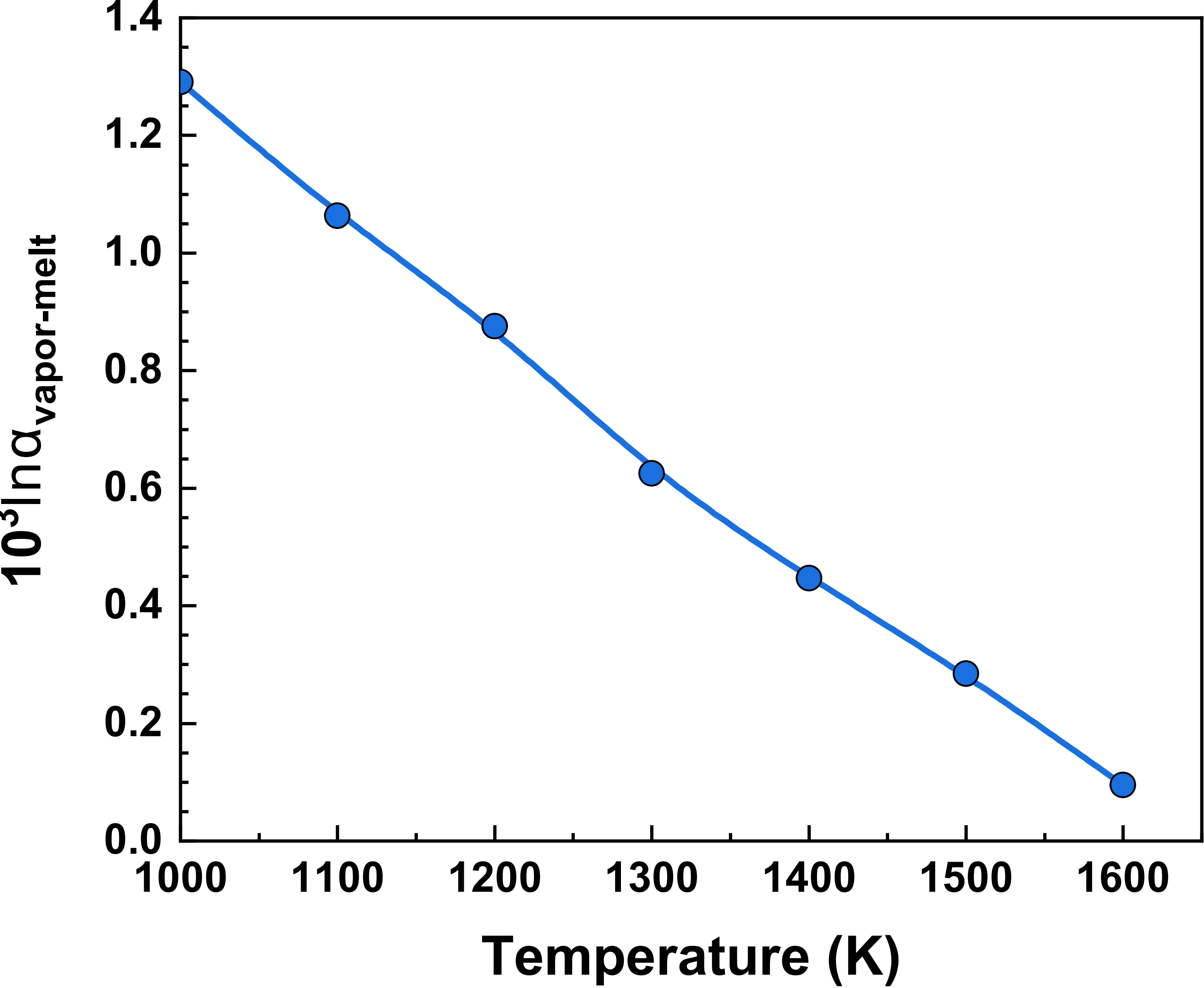

$10^3\ln\alpha_{vapor\text{-}melt}$
1.4
1.2
1.0
0.8
0.6
0.4
0.2
0.0
1000
1100
1200
1300
1400
1500
1600
Temperature (K)